

Full paper

Optimal annealing of Al foil anode for prelithiation and full-cell cycling in Li-ion battery: The role of grain boundaries in lithiation/delithiation ductility

Yue Yu^{a,b}, Sa Li^{a,b,**}, Huimin Fan^{a,b}, Hui Xu^{a,b}, Mengwen Jiang^{a,b}, Yunhui Huang^{a,b}, Ju Li^{c,*}

^a School of Materials Science and Engineering, Tongji University, Shanghai, 201804, China

^b Institute of New Energy for Vehicles, Tongji University, Shanghai, 201804, China

^c Department of Nuclear Science and Engineering and Department of Materials Science and Engineering, Massachusetts Institute of Technology, Cambridge, MA, 02139, USA



ARTICLE INFO

Keywords:

Metallic foil anodes
Mechanical prelithiation
Heat treatment
Lithiation/delithiation ductility
Electronic percolation
electrochemical complexation of grain boundary

ABSTRACT

While self-supporting Al foil anode has high theoretical capacity and appropriate potential for Li-ion batteries, the poor initial Coulombic efficiency (ICE) retards its wide industrial applications, making prelithiation necessary. Herein, we develop a facile and efficient mechanical prelithiation (MP) approach suitable for mass production. Even though ICE was improved from 70% to 90% after MP, the cycling performance is still deficient, which we attribute to the insufficient density of grain boundaries that leads to poor lithiation/delithiation ductility (LDD), characterized by the rapid loss in electronic percolation across the foil. As a classic strategy in metallurgy to tune the grain boundaries, thermal annealing and recrystallization is further exploited to optimize the LDD of Al foil. For standard Al foil, whose grain size is big with lots of dislocations inside, MP followed by electrochemical cycling causes cracking, electrolyte infiltration and SEI formation. Its electronic percolation (damage) is monitored in real time, and is found to decay rapidly as the insulating SEI blocked all the electron transport paths of one grain (or a cluster of grains). But if MP takes place after annealing standard Al foil at 300 °C for 15min, the dislocations recombined to achieve refined grains whose sharp GB network can slide effectively to relieve stress buildup due to phase transitions and suppress deep crack development, and the prelithiated foil achieved superior electrochemical performance, with significant life extension in the in-plane electronic conductance. However, interestingly, upon further increase in the annealing temperature, as the grain size turns bigger, the electrochemical performance of prelithiated foil deteriorates. Based on the comparison of the microstructures and electrochemical performance at different thermal annealing conditions, we found that the GB density before MP plays an essential role in the stress relief and keeping electronic percolation during cycling. Our optimized prelithiated Al foil maintains 80% capacity retention after 100 cycles in LiFePO₄//LiAl_y full cell with 1.8 × excess lithium. It cycles significantly better than pure Li_{BCC} foil of equal thickness (65 μm), especially in lean-electrolyte condition, suggesting such safe, cheap and high energy density metallic foil anodes deserve comparable attention as pure lithium metal anode.

1. Introduction

Aluminum should be an attractive alloying-reaction anode for Li-ion batteries considering its high theoretical gravimetric capacity (2235 mAh g⁻¹ if lithiated to Li₉Al₄), appropriate electrochemical potential plateau (~0.2 V vs. Li⁺/Li) and low cost (~\$2000/ton) [1]. While prevailing researches have been focused on Al nanoparticles and

slurry-based blade-casting technique [2], the high surface area of powders, especially nano-powders, would inevitably aid detrimental side reactions, consuming both active lithium and electrolyte. Besides, regarding the conventional slurry-based preparation process, the introduction of inactive components, such as conductive agent, binder and current collector, would also decrease the practical energy density [3,4]. Therefore, free-standing Al foil that eliminates inactive components,

* Corresponding author.

** Corresponding author. School of Materials Science and Engineering, Tongji University, Shanghai, 201804, China.

E-mail address: liju@mit.edu (J. Li).

<https://doi.org/10.1016/j.nanoen.2019.104274>

Received 14 September 2019; Received in revised form 23 October 2019; Accepted 5 November 2019

Available online 9 November 2019

2211-2855/© 2019 Elsevier Ltd. All rights reserved.

slurry preparation, and blade-casting procedure, should be attractive for industrial applications. Unfortunately, previous attempts using self-supporting Al foil anodes revealed that the initial Coulombic efficiency (ICE) is quite poor (Fig. S1), generally around 70%. As a result, prelithiation is necessary if it is to have any chance to be used in practical full cells with limited Li inventory. A prelithiated free-standing LiAl_y (average composition) foil can be directly compared to the popular pure Li metal foil used in Li-metal batteries (LMB). Their performances in full cells should be contrasted on equal foil thickness (for comparing volumetric energy density), or equal foil weight (for gravimetric energy density), footing. With a typical industrial-level cathode areal capacity of $\sim 2.65 \text{ mAh cm}^{-2}$ (single side), the anode foil thickness should be on the order of $\sim 50 \mu\text{m}$ (single side) to be competitive against graphite anode in volumetric energy density. The amount of excess Li inventory contained in a pure Li_{BCC} foil anode ($y=0$) of $50 \mu\text{m}$ thickness is 10 mAh cm^{-2} , while a LiAl foil ($y=1$) of $50 \mu\text{m}$ thickness contains excess Li of 6.9 mAh cm^{-2} which is comparable. The number of full-cell cycles one can run with such limited Li inventory is the key

figure-of-merit for any metallic foil anodes including pure Li foil. It is also important to keep in mind that as long as the anode potential stays above $\sim 0.2 \text{ V}$ vs. Li^+/Li , thermodynamically there is no possibility of precipitating out Li metal which is in the body-centered cubic (BCC) phase (Li_{BCC}), thus eliminating the possibility of Li_{BCC} dendrites, an essential problem for LMBs that is both a safety concern and a cause for poor Coulombic efficiency [5]. Also, the evolution of structural damage in the metallic foil with cycling, in the form of porosities, cracks, solid-electrolyte interphases (SEI) (which must form at such low potentials whenever liquid electrolyte touches any electron-donating metallic surface), and dead particles surrounded by insulating SEIs, are expected to be different, as Li_{BCC} and intermetallic compounds LiAl and Li_9Al_4 are very different metals from a fundamental perspective. For a metallic foil anode which does not carry other conductive agent (like carbon black in slurry electrodes), but with insulating agents (SEI and SEI debris) mixed in with cycling, maintaining electronic percolation is key. *A priori*, it is not clear that a free-standing LiAl_y foil should lose to pure Li_{BCC} foil in real performance comparisons. Indeed, our paper will

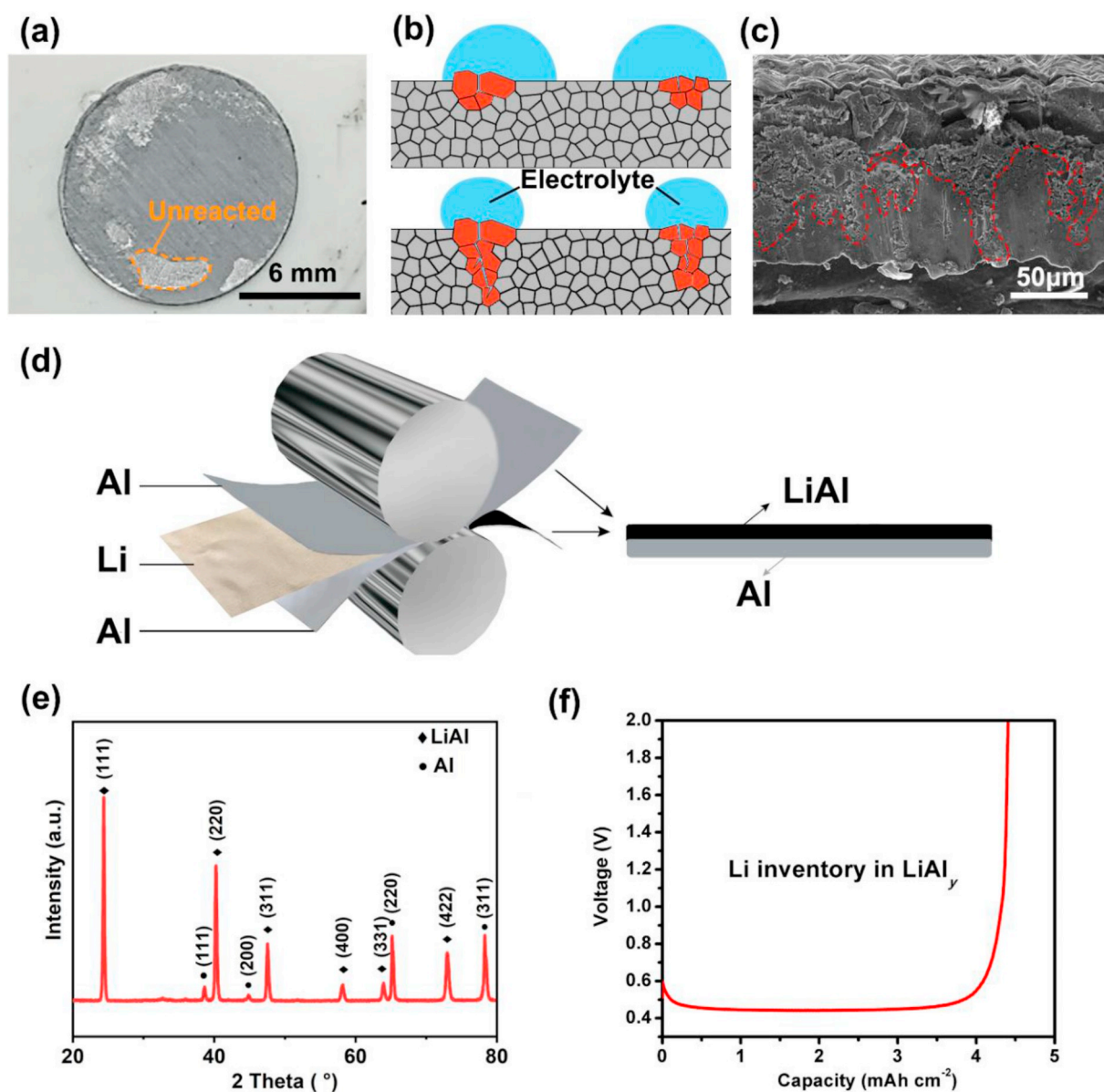


Fig. 1. Electrolyte localization and the preparation of LiAl_y foil. a) The optical photograph of Al foil after electrochemical prelithiation. b) Schematic illustration of electrolyte localization. c) The cross-sectional SEM image of Al foil treated by electrochemical prelithiation. d) Schematic illustration of mechanical prelithiation (MP). e) XRD characterization and (f) the voltage-capacity curve of Al treated by mechanical prelithiation.

show that LiAl_y foil is generally superior to pure Li_{BCC} foil in full cell performance, and therefore deserves comparable attention as the very popular LMB configuration.

Several prelithiation approaches such as stabilized lithium metal powder (SLMP) [6], lithiated Si powder [7], Li-rich cathode additive [8], and electrochemical prelithiation method have been developed to compensate for active lithium loss in subsequent electrochemical cycling. The aforementioned prelithiation methods aimed at slurry-based preparation, and it seems only electrochemical prelithiation is applicable to metallic foil anodes. Generally speaking, when performing electrochemical prelithiation, one needs to firstly lithiate the electrode in a working cell against Li metal as a sacrificial source and then disassemble the cell, followed by washing away the residual electrolyte. But such a prelithiation procedure is likely too complex for large-scale production. Done at lab-scale and coin cell level, Al foil also has big problem with maintaining good wetting with liquid electrolyte [9] and severe electrolyte localization (EL) often occurs, causing spatially inhomogeneous prelithiation (Fig. 1a). Even worse, such inhomogeneity would be amplified in the following full-cell cycling, considering the prelithiated regions have better electrolyte wettability (we will prove this in Fig. 2). Note that EL is an auto-catalytic process, which means region in contact with more liquid electrolyte is more active during cycling, leading to more pulverization, and thus absorbing even more electrolyte, while other regions are deprived of liquid electrolyte and barely contribute capacity. Al foil hence will be penetrated in the electrolyte-localized regions as if corroded (illustrated in Fig. 1b and demonstrated in Fig. 1c), which is exacerbated by poor electrolyte wetting before electrochemical prelithiation [9]. A more homogeneous prelithiation technique that is designed for metallic foil anode is desperately needed.

Here we develop a mechanical prelithiation (MP) method (Fig. 1d), utilizing reactive bonding between Li_{BCC} and Al_{FCC} that can take place at room temperature:



where LiAl_{cubic} is an intermetallic phase that can be clearly identified by XRD (Fig. 1e) afterwards, although generally speaking we do not exclude the possibility of other “Li-rich” products [10]. We sandwich a single 50 μm thick Li_{BCC} foil between two 93 μm thick Al_{FCC} foils, and use a roller to force the reaction, as Fig. 1d shows. On each side, the reaction forms a ~44.2 μm thick LiAl_{cubic} layer on top of a ~68.4 μm thick layer of residual unreacted Al_{FCC}. Since LiAl_{cubic} is quite brittle, we can easily mechanically peel off the two layers after all Li_{BCC} sandwiched in the middle are consumed, and obtain two LiAl_{cubic}/Al_{FCC} sheets, that can act as free-standing anode. Because there is almost no difference between the reaction conditions of the 2 sides, including the same reaction interfaces (Li/Al interface), and a pair of symmetrical forces by the roller, so that the two LiAl_{cubic}/Al_{FCC} sheets would have almost the same average thickness and physical/electrochemical properties. To determine the lithium inventory, we assembled LiAl_y//Li half cell by paring Li metal anode (12 mm diameter) against the LiAl_y electrode (12 mm diameter) and then delithiated to 2.0 V at a current density of 1 mA cm⁻². From Fig. 1f, 4.65 mAh cm⁻² lithium could be extracted, approximately the areal capacity equivalent of 25 μm thick (50 μm thick Li_{BCC} foil for two 93 μm thick Al_{FCC} foils) Li_{BCC} foil (5.15 mAh cm⁻² = 3860 mAh g⁻¹ × 0.534 g cm⁻³ × 25 μm), which confirmed metallurgical prelithiation is an effective prelithiation method. In a full cell with a cathode such as LiFePO₄ which comes with a full complement of Li, when it is first charged, the cathode’s lithium will be transported and deposited on the metallic foil anode. So, the 44.2 μm thick LiAl_{cubic}/68.4 μm thick Al_{FCC} will be further lithiated, with the LiAl_{cubic} layer thickening beyond 44.2 μm and the Al_{FCC} layer shrinking below 68.4 μm. In the next half-cycle (discharging), this will be reversed, as a full complement of Li will be returned to the cathode and some LiAl_{cubic} reverts back to Al_{FCC}.

Whether in the initial mechanical lithiation, or in subsequent electrochemical lithiation/delithiation with electrolytes, there are two persistent materials science questions: (a) how is lithium mass transported, namely, through grain boundary network, dislocation cores or bulk lattice of the metallic phases, and/or via cracks in-filled with liquid electrolyte and SEI, and (b) how does the Al_{FCC}↔LiAl_{cubic} phase transformation occur, what controls the reversibility of such phase transformations with volume change up to 195%, and what preprocessing steps can affect the damage tolerance of the metallic foil in electrochemical cycling, by for example, controlling the initial grain size. It is important to keep in mind that during electrochemical lithiation/delithiation, the question of *electronic percolation* is paramount, as in any half-cell reaction:



e⁻(metal) needs a percolating path to the external circuit for reaction (2) to continue cycle after cycle. Electronic percolation is by no means a trivial problem when the metallic foil starts to crack and becomes in-filled with liquid electrolyte and SEI, both electronic insulators. In other words, the foil is gradually turning into a metallic-insulator composite.

The question of electronic percolation to the active metal (A or B) is intimately related to the “damage state” of the metallic foil. If we take A to be a metallic grain, then e⁻(metal) comes to A by hopping across grain boundary (GB), as grains are all surrounded by GBs. A is connected to multiple adjacent grains via corresponding GBs, and initially all of these GBs have no problem allowing e⁻(metal) to conduct across. However, with repeated volume expansion and shrinkage, some of these GBs can come apart, allowing partial or complete liquid electrolyte infiltration. This would decrease the ability of e⁻(metal) to hop across this GB (while simultaneously increasing the lithium mass transport ability *along* the GB). We call such transformation a change in the *electrochemical complexion* of the GB. The extreme limit of a complexion change would be the GB completely cracking open, with thick enough SEIs forming on both sides and liquid electrolyte in between that completely shut off electron tunneling, but we can also have all kinds of gradations in between, such as (a) gentle GB sliding induces extra free-volume to allow faster Li atom (neutral) GB diffusion, while the GB still maintains metallic contact, or (b) the GB had opened up a few Angstroms, losing ability to sustain tensile loading, but has later closed up under compressive stress, and the SEI residuals are still quite thin to allow electron tunneling across, etc. We can systematically classify GB complexion by its ability to conduct e⁻(metal) across, Li mass along, and the ability to sustain tensile and shear stress across a particular GB. The general trend must be however, with repeated phase transformations, free volume↑, GB Li mass diffusivity↑, e⁻(metal) hopping across↓ and load bearing ability↓.

Initially, with only a few GBs transformed, A would not lose electronic percolation, since e⁻(metal) can come through other less damaged GBs. Indeed, the electrochemical kinetics may even improve for A temporarily, since it will have better access to Li⁺(electrolyte) via the few cracked and infiltrated GBs, while e⁻(metal) can still come from the remaining intact GBs. However, with stress/volume evolution and damage accumulation, as grain A becomes entirely surrounded by GBs with altered electrochemical complexion that disfavors e⁻(metal) transport, grain A would become electronically deactivated and becomes a “flotsam” or “dead particle” surrounded entirely by SEI and/or liquid electrolyte.

When we inspect the necessary ingredients for (2), complementary to e⁻(metal) percolation, there can also be a concern for Li⁺(electrolyte) and electrolyte percolation, especially when the liquid electrolyte is near dry-out in some places. Because liquid can flow, as long as we have superabundant liquid electrolyte in the cell, the state of health of the ionic conduction should not be a problem. But in practical full cells in industry, the amount of liquid electrolyte used is often very limited, and

liquid electrolyte dry-out can be a real bottleneck. The previously mentioned electrolyte localization (EL) [9] in cycled coin cells suffers from liquid electrolyte dry-out and Li^+ (electrolyte) percolation problems (Fig. 1a) eventually.

In this paper, we focus on preprocessing of Al foil before the mechanical prelithiation (MP) step, that we find can positively affect its lithiation/delithiation ductility (LDD) later, that is, the ability of the metallic foil anode to maintain electronic percolation so reaction (2) can happen repeatedly, despite dramatic thickness changes. In previous work with mechanical shot-peening pretreatment, we found that smaller grain size seems to improve LDD. This may be understood by Weibull statistics argument [11,12]. If we think about the total area of damaged GBs that is required to completely electronically isolate all the grains in a 93 μm thick foil, then a metallic foil with coarse grains will require less total area of cracked GBs than a fine-grained metallic foil. In other words, with coarse grains, one is putting “more eggs in one basket”; with fine grains, even if certain grain loses electronic percolation, one loses a smaller fraction of the active metal. Furthermore, we hypothesize that GB sliding is an important stress-relief mechanism to accommodate the phase transformation strains, so denser GB network allows better stress relief globally and reduce the tendency to cracking and electrolyte infiltration.

However, in the previous paper, while shot-peening treatment refines the Al_{FCC} grains, one also introduces more dislocations. Dislocations, in principle, are also short-circuit diffusion paths for Li mass transport (even though they are less likely to crack open after Li atom insertion). So, their role needs to be clarified. In the present work, we have performed two kinds of heat treatment [13] on Al_{FCC} foil before the prelithiation. The Al_{FCC} foil are produced by rolling and comes with lots of stored dislocations. Both heat treatments reduce the dislocation density monotonically, but while the heat treatment at intermediate temperature (IHT) refines the grains and increases the sharpness of the GBs (recrystallization and polygonization), the higher-temperature heat treatment (HHT) coarsens the grains. We find IHT improves electrochemical ductility significantly, while HHT improves electrochemical ductility compared to as-received (AR) sample without heat treatment, but degrades it compared to IHT, proving that sharp 2D grain boundaries, rather than dislocation tangles, are more essential for improving the lithiation/delithiation ductility.

2. Experimental

2.1. Materials preparation

AR Al foil (99.9999%, 93 μm) was put it in muffle furnace at 300 °C or 500 °C for 15min. Then we cooled it in air to obtain the IHT and HHT Al foil. Roll-to-roll prelithiation was carried out on the AR, IHT and HHT Al foil respectively. One piece of 50 μm Li foil (China Energy Lithium Co., Ltd.) was sandwiched between two Al foils and they were rolled with a roller (MSK-2150, Shenzhen Kejing Star Technology, Ltd.) in the dry room. Then we obtained LiAl_y foils and they were punched into disks with a diameter of 12 mm as the anode in coin cell. Commercial LiFePO_4 cathode ($\sim 2.65 \text{ mAh cm}^{-2}$) with 12 mm diameter was paired against the LiAl_y in the full cell and the Li metal was used in the half cell. The 9 cm^2 (3 cm \times 3 cm) square of double-sided lithiated Al foils (130 μm for double-side use and thus 65 μm single side) and the Li foils (equal area and thickness with the double-sided lithiated Al foil) were used as anode in the pouch cell. The commercial LiFePO_4 ($\sim 2.65 \text{ mAh cm}^{-2}$) was punched into a 9 cm^2 (3 cm \times 3 cm) square as cathode in the pouch cell. The commercial electrolyte (EC/DEC v/v = 1:1 with 10 wt% FEC and 1 wt% VC as additives) was used. The pouch cell paired with three battery tabs (two on LiAl_y anode and one on LiFePO_4 cathode) was used as a three-electrode pouch cell prototype to test the in-operando electronic percolation.

2.2. Electrochemical measurement

The CR2025-type coin cells were assembled in the glove box (water $< 0.1 \text{ ppm}$, $\text{O}_2 < 0.1 \text{ ppm}$) with 60 μL commercial electrolyte, and their electrochemical performance were carried out by Neware test system (CT-4008, Neware). The $\text{LiFePO}_4//\text{Al}$ and $\text{LiFePO}_4//\text{LiAl}_y$ full cells were tested between 2.0 V to 3.8 V at a current density of 1 mA cm^{-2} . The $\text{LiAl}_y//\text{Li}$ half cell was delithiated to 2.0 V at a current density of 1 mA cm^{-2} . The pouch cells were assembled in the dry room with 8g Ah^{-1} commercial electrolyte. The electrochemical test on the $\text{LiFePO}_4//\text{LiAl}_y$ pouch cells were carried out between 2.0–3.8 V and the $\text{LiFePO}_4//\text{Li}$ pouch cells were carried out between 2.3–4.1 V at the rate of 1C (based on cathode). The cyclic voltammetry (CV) was conducted by CHI660E electrochemical workstation at different scan rates ranging from 0.01–0.1 mV s^{-1} at a potential range of 0–1.5 V versus Li^+/Li (CHI660E, Shanghai Chen Hua Instrument Co., Ltd.). As for electronic percolation test, we apply a small voltage bias across the two battery tabs of the LiAl_y anode every two cycles, calculating the resistance across the anode foil by reading the current from the multimeter (Ohm's Law).

2.3. Characterizations

The surface and cross-sectional morphologies of the metal foil anode were performed by field emission scanning electron microscope (SEM, FEI Quanta 250FEG) under an accelerating voltage of 10 kV. The XRD characterization were carried out on a Bruker D8-Advance powder X-ray diffractometer operated at 40 kV and 30 mA, using $\text{Cu K}\alpha$ radiation ($\lambda = 0.15405 \text{ nm}$). The electron backscattered diffraction (EBSD) characterization was carried out at acceleration voltage of 20 kV with a beam current of 17 nA (Nordlys F+, Shanghai Oxford Instruments Co., Ltd.).

3. Results and discussion

In this study, we develop a facile and efficient roll-to-roll mechanical prelithiation (MP) approach, which is suitable for mass production and requires no electrolyte to assist. By sandwiching one layer of 50 μm thick Li foil between two 93 μm thick Al foils and then pressing by a roller, we achieve full solid-state reactions at room-temperature that completely “absorb” the 50 μm thick Li_{BCC} into the two sides, forming intermetallic compounds LiAl on both sides. Note that formation process of LiAl_y is quite rapid, which may be sped up with the aid of rolling pressure, because of the increased true contact area between the two reacting metals. As revealed in Fig. S2, when 30 MPa pressure is applied in this study, the black LiAl_y product appears in some regions within 1s. With prolonged pressing time, more and more black LiAl_y product is generated, and one could observe the surface completely turns to black in 10s, indicating a rather fast formation of LiAl_y . However, while under 10 MPa pressure for 10s, one only gets scattered and fragmentary LiAl_y , separated by the unreacted regions as shown in Fig. S3.

Because these LiAl are hard and brittle, and the remaining trace amount of Li_{BCC} are easy to rupture, so upon mechanical peeling, the two originally 93 μm thick Al foils (now $\sim 115.5 \mu\text{m}$ thick LiAl/Al foils) cleanly separate into two pieces, with surface roughness $\sim 29 \mu\text{m}$ (maximum height of the profile). The 50 μm thick Li_{BCC} has disappeared, being completely absorbed. The thus-obtained two LiAl/Al sheets can then serve as free-standing anodes, as demonstrated in Fig. 1d. Although the LiAl phase is very thick and brittle, we find such LiAl layer is toughly adhering to the underlying unreacted Al and cannot peel off even after harsh bending and winding, as revealed in Fig. S4 and Movie S1, and supported by the unreacted Al, the prelithiated layer could maintain intact in the bending and winding test.

Interestingly, after alloying with lithium, the liquid electrolyte wettability of the foil is significantly improved, and the contact angle is reduced from 30.8° to 13.6°. In previous work we found there was significant electrochemical noncontact areas (ECA) on AR Al foil (supplied by Qinghe County Xingye Metal Materials Co., Ltd.) when assembled in

coin cells using common carbonate electrolyte due to poor contact angle [9], which inevitably renders some Al foil regions non-reacting and causes subsequent electrolyte localization, which greatly deteriorates electrochemical performance by ever-more non-uniform lithiation. Even worse, such inhomogeneity would be amplified in the prolonged full-cell cycling, causing damage accumulation until the Al foil are completely perforated (leaking electrolyte through) as if in localized corrosion. Therefore, more uniform lithiation/delithiation is expected from mechanically prelithiated LiAl/Al foil anode due to reduced electrolyte contact angle.

However, surface SEM images of the LiAl/Al sheets before any electrochemical cycling still reveal huge cracks $\sim 4\ \mu\text{m}$ wide, as shown in Fig. 2c. From cross-sectional SEM in Fig. 2d, it is found the fracture could be as deep as $\sim 45\ \mu\text{m}$. Such broad, deep and far-extending cracks would store electrolyte like finger lakes, inducing EL and crumbling of the foil anodes as discussed above. With electrolyte imbibition, insulating SEI will gradually build up. Once a grain becomes surrounded entirely by electronically insulating SEI, it would become deactivated, leading to capacity loss. Therefore, one needs to eliminate such broad, deep and far-extending fracture as much as possible in the first place. Such cracking damage generated during MP is one manifestation of the poor LDD of the AR Al foil, which was formed by cold-rolling. The AR Al foil has plenty of stored dislocations in the form of diffuse dislocation tangles, but not a lot of sharp GBs. These 1D dislocations are apparently not able to relieve the stress generated by MP. That is to say, due to ineffective mechanisms to relieve stress, the AR Al foil cannot accommodate massive lithiation shock, and some of its GBs would come apart completely, forming cracks. Later, after injection of organic electrolyte, we found the LiAl/Al foil anode will also constantly suffer from the same poor LDD during subsequent electrochemical lithiation/delithiation. Hence, an approach to improve the LDD of LiAl_y foil (y is the average degree of lithiation in one foil) is needed.

From our previous work [14] it is found that grain refinement allows better stress relief globally and reduce the tendency to cracking and electrolyte infiltration, which prompt us to speculate that sharp GB network would improve LDD. Through Weibull statistics argument, we

speculate that metallic foil with coarse grains has a greater risk of becoming electronically isolated for it requires less total area of damaged GB to block all electronic percolation paths. Therefore, thermal annealing, as a classic strategy to tune GBs, is adopted to optimize Al foil here before MP and full-cell cycling. The AR Al foil comes with a lot of dislocation tangles. At annealing temperatures higher than $0.35T_m$, dislocations can rearrange into sharper (sub-)grain boundaries (polygonization), or, can provide nucleation opportunities to form completely new grains (recrystallization) to eliminate both residual stress and dislocation core energies. Experimentally, we anneal the Al foil at $300\ ^\circ\text{C}$ (intermediate, IHT) or $500\ ^\circ\text{C}$ (high, HHT) for 15min, respectively, before carrying out MP. Electron backscattering diffraction (EBSD) characterization shows the coarse grains of the AR Al foil (Fig. 3a) with some diffuse GBs. With intermediate annealing of $300\ ^\circ\text{C}$, recrystallization and polygonization are initiated to refine the grains and increase the sharpness of the GBs (Fig. 3b). However, if the annealing is $500\ ^\circ\text{C}$ for 15min, the grains will end up coarser than $300\ ^\circ\text{C}$ annealed due to activation of grain growth after polygonization/recrystallization (Fig. 3c), although the grain boundaries are much sharper than unannealed sample, and the grain size is also still somewhat smaller than the unannealed sample. After performing MP, morphological inspections show that either heat treatment improves the LDD of the foil, which is consistent with the foregoing discussion that dense, sharp GB network allows more GB sliding systems to work and relieve phase transformation stresses. No huge crack could be observed visually on the surface (Fig. 3d) and a uniform reaction layer is found from the cross-sectional SEM image (Fig. 3e) of the IHT + MP sample. The grain size of as-formed LiAl_y in AR, IHT and HHT samples is further examined through XRD, which interestingly exhibits a similar ranking of pristine grains before MP, as revealed in Fig. S5.

Note that the average thickness of the reacted layer of the IHT + MP sample is $61.1\ \mu\text{m}$ (Fig. 3e), 38% deeper than that of AR + MP foil (about $44.2\ \mu\text{m}$, Fig. 2d), even though both IHT + MP and AR + MP samples fully absorbed the same amount lithium ($50/2=25\ \mu\text{m}$ worth of Li_{BCC}). From *ab initio* calculations (materialsproject.org), Li_{BCC} (mp-135) has volume per Li atom of $20.121\ \text{\AA}^3$, Al_{FCC} (mp-134) has volume per Al

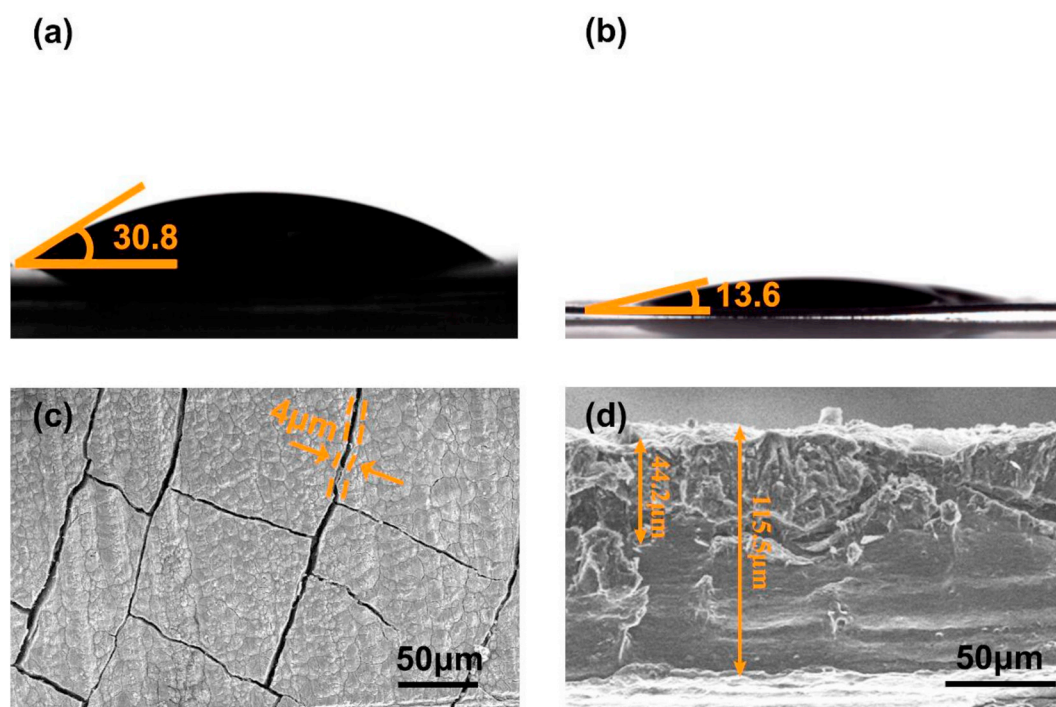


Fig. 2. The liquid electrolyte wettability (optical) and SEM images of AR + MP sample. The contact angle of (a) AR and (b) AR + MP sample. (c) Top-view SEM and (d) cross-sectional SEM images of AR + MP sample.

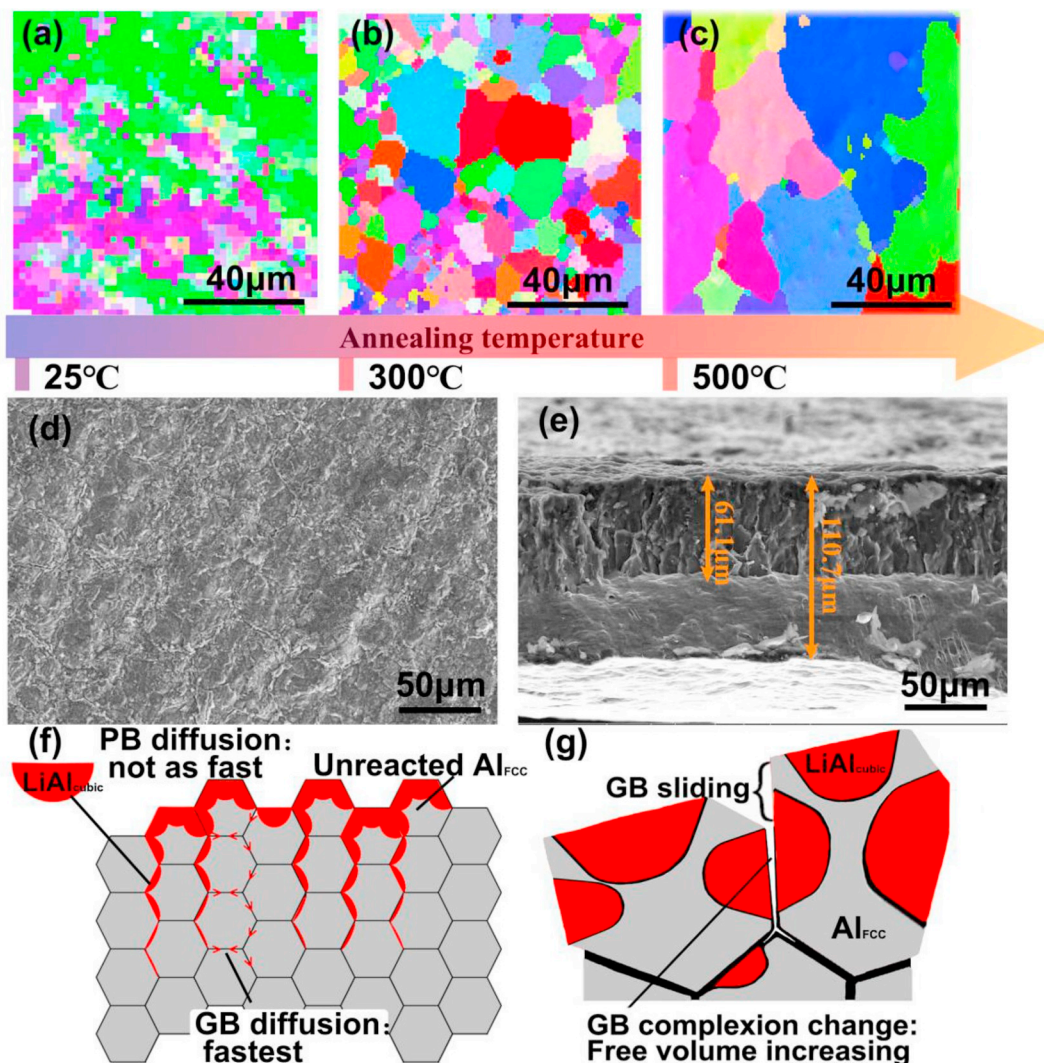


Fig. 3. EBSD and SEM images. The EBSD images of the (a) AR, (b) IHT and (c) HHT Al foil. d) Top-view SEM and (e) cross-sectional SEM images of IHT + MP LiAl₃ foil. f) Illustration of Li atomic diffusion and g) the change of the GB complexion during MP.

atom of 16.472 \AA^3 , and LiAl_{cubic} (mp-1067) has volume per LiAl of 32.103 \AA^3 . So to absorb 25 \mu m worth of Li_{BCC}, at least $(16.472/20.121) \times 25 \text{ \mu m} = 20.47 \text{ \mu m}$ worth of Al_{FCC} is needed for the reaction, forming 39.887 \mu m worth of LiAl_{cubic}. This agrees well with the observed geometry of the AR + MP sample (about 44.2 \mu m reacted layer, Fig. 2d), which means the reacted layer of the AR + MP contains mostly LiAl_{cubic} with at most a small minority of unreacted Al_{FCC} phase mixed in. However, with the IHT + MP sample, the phase mixture *within* the reacted layer is far different: at least $10\text{--}30 \text{ \mu m}$ worth of residual unreacted Al_{FCC} phase must be mixed in with the 39.887 \mu m worth of LiAl_{cubic} (which is the hard and brittle phase). So the reaction layer in IHT + MP sample must be LiAl_{cubic}/Al_{FCC} composite instead of the purely LiAl_{cubic} layer of the AR + MP sample, with significant volume fraction of Al_{FCC} phase. This situation is quite similar to “retained austenite” in martensitic phase transformation of steel, where the brittle martensite phase is mixed with ductile residual (untransformed) austenite phase, that significantly improves the overall ductility of the quenched steel. Since LiAl_{cubic} is a quite brittle phase, we think the significant residual Al_{FCC} in the 61.1 \mu m reaction layer is of great help for improving LDD.

We then need to explain why the MP reaction layer is so much deeper in IHT + MP than AR + MP, and why there is so much unreacted Al_{FCC} phase within it. Since IHT + MP has less dislocations than AR + MP, the deeper reaction layer cannot be caused by short-circuit diffusion in

dislocation cores (aka pipe diffusion) [15]. Indeed, the net defect population (as defined by total free-energy excess) monotonically decreases with annealing. Thus, it must be that the spatial organization of defects that make the difference here, not the total amount. Specifically for dislocations and grain boundaries: it is well known that grain boundary is a special organization form of geometrically necessary dislocations (GND) [16]. The total dislocation density, consisting of statistically stored dislocations (SSD) and GND densities, monotonically decreases with annealing. Our experimental observations indicate that when the stored dislocations reorganize into sharp GBs, the GB network facilitate the deeper reaction. Indeed, we believe GB diffusion is the fastest diffusion path in MP, and the lithium atoms prefer to migrate along GBs than any other paths (phase boundaries, dislocation cores, or lattice). Since the 2D GBs form a percolating network in the foil, they facilitate deep invasion of the Al_{FCC} → LiAl_{cubic} phase transformation, as transformation *into* the grain is relatively sluggish (which already takes advantage of the incoherent LiAl_{cubic}/Al_{FCC} phase boundary as illustrated in Fig. 3f). In addition, due to the GB density in HHT + MP sample is lower than IHT + MP, we observed its reaction layer (Fig. S6) also correspondingly thinned (about 55 \mu m), namely, the reaction layer thickness order is IHT + MP > HHT + MP > AR + MP. This is very consistent with what we discussed above.

We can further speculate why GB diffusion is faster than incoherent phase boundary (PB) diffusion or dislocation core diffusion. The reason

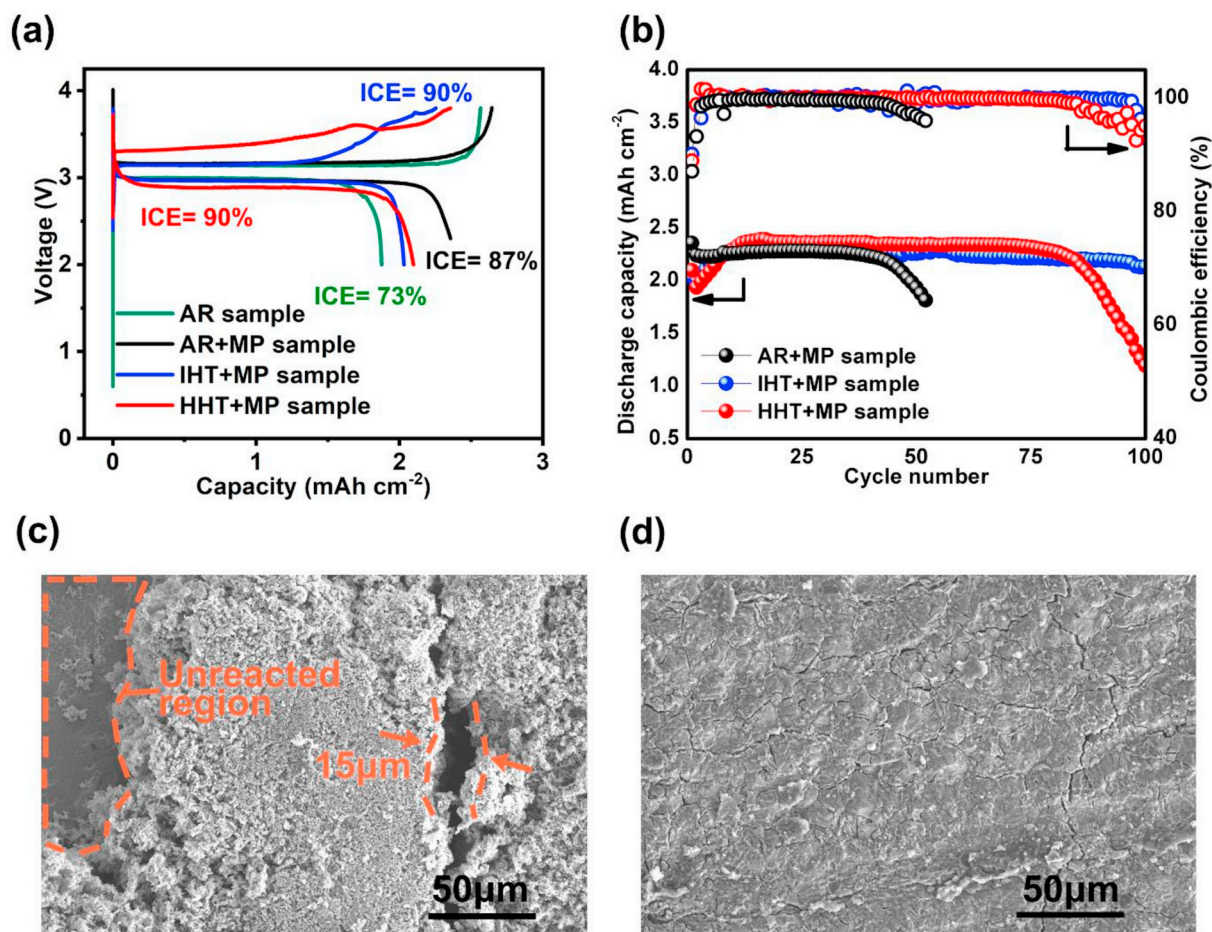


Fig. 4. Electrochemical properties, and the SEM images of the anode after cycling. a) The voltage-capacity curve of LiFePO₄ cathode versus AR, AR + MP, IHT + MP and HHT + MP anode in the first cycle. b) Comparison of the discharge capacity and Coulombic efficiency of the AR + MP, IHT + MP and HHT + MP sample. The SEM images of (c) AR + MP and (d) IHT + MP sample after 40 cycles in LiFePO₄/LiAl_y full cell.

is likely mechanical and has to do with free-volume evolution. As illustrated in Fig. 3g, the diffusion pathways of Li atoms in a metal can be its GBs, phase boundaries, dislocations or even the bulk lattice. However, ongoing phase transition will alter the GB complex, when the Al–Al GBs is changed to LiAl–Al or LiAl–LiAl GBs, with violent GB sliding. Therefore, the GB free volume will increase *in situ* so that the Li diffusion ability along the GBs will be continuously enhanced for future Li invasion. In contrast, for Li atom diffusion in LiAl/Al PB (which should also have incoherent atomic structures), their interfacial complex is not going to change much with the enlargement of the LiAl domain and shrinkage of the Al domain, as the PB moves vertical to itself and its nature is relatively invariant, so that it keeps a relatively low diffusion ability compared to the sliding GBs. This causes the Li atom to diffuse faster along the GBs than transformation inside the grain based on PB diffusion. The IHT + MP sample (Fig. 3b) has more GBs to provide faster Li diffusion pathway into the foil. Even when a grain is not fully lithiated inside, other Li atoms can pass over it along GBs (Fig. 3f) and to start lithiation of the next grain. By the time the 25 μm worth of Li_{BCC} has been consumed, there are still unreacted Al_{FCC} phase within individual grains, which indicates the relative sluggishness of PB diffusion. For further confirmation, we scratched some LiAl_y fragments (Fig. S7a) and examined the composition through X-ray diffraction. From Fig. S7b, both the LiAl peak and Al peak can be detected, verifying that there is some residual metallic Al in the prelithiated layer. Here, since both IHT and HHT heat treatments have improved the LDD while reducing the dislocation density monotonically, we conclude that the sharp GBs, instead of dislocations, are essential to get better LDD

compared to AR sample. The role of GBs and dislocation will be further clarified later, when we contrast the LDD of HHT + MP sample with IHT + MP sample quantitatively with electrochemical cycling.

The thicknesses of the AR, AR + MP, IHT + MP and HHT + MP samples are measured and shown in Table 1. The total thickness is decomposed into the reacted layer thickness and the unreacted layer thickness $t_{\text{total}} = t_{\text{react}} + t_{\text{unrea}}$. Independent measurements are performed at different locations of the foil to not only obtain the average $E[t]$, but also the standard deviation $\sigma[t]$ (the value behind the \pm in Table 1). Note that when measuring the t_{react} and t_{unrea} , randomly 30 spots were selected from a random but typical cross-sectional SEM image. Take AR + MP sample as an example (shown in Fig. S8), the t_{react} is measured as shown in Table S1, based on which the average and variation are obtained. For IHT + MP and HHT + MP samples, similar approach is used to calculate t_{react} and t_{unrea} . Interestingly, all the total thickness of AR + MP, IHT + MP and HHT + MP deviate from the theoretical value that is supposed to be 112.4 μm (39.887 μm LiAl +

Table 1
Measured thickness of the AR, AR + MP, IHT + MP and HHT + MP samples.

Thickness[μm]	Sample			
	AR	AR + MP	IHT + MP	HHT + MP
Total thickness t_{total}	93.1 ± 0.9	115.5 ± 5.2	110.7 ± 4.2	109.8 ± 3.0
Reacted layer thickness	/	44.2 ± 7.2	61.1 ± 1.3	55.2 ± 1.3
t_{react}				
Unreacted layer thickness t_{unrea}	/	68.4 ± 7.5	51.8 ± 4.7	55.1 ± 5.1

72.513 $\mu\text{m Al}_{\text{FCC}}$ after reacting 93.1 $\mu\text{m Al}$ foil with 25 $\mu\text{m Li}$ foil. While the positive deviation of $t_{\text{total}}(\text{AR} + \text{MP})$ from 112.4 μm may be attributed to the porosity that is caused by the lithiation shock damage during the MP process, as revealed in Fig. 2c and d, and can be used as a quantitative measure of “free volume” and “damage”, it is puzzling why $t_{\text{total}}(\text{IHT} + \text{MP})$ and $t_{\text{total}}(\text{HHT} + \text{MP})$ are slightly smaller than 112.4 μm . We then discovered that there is lateral areal expansion in the foil after MP (see Fig. S9): for example, the area of IHT + MP is 115.5% (see Table S2) the area of the IHT sample before MP (which is \approx area of the AR sample). There is clear sample-wide plastic deformation in both in-plane x,y and out-of-plane z during MP. We therefore define

$$\alpha \equiv \text{area}(\text{after MP}) / \text{area}(\text{before MP}) \quad (3)$$

and then calculate a corrected porosity damage within the reacted layer:

$$p \equiv (E[t_{\text{total}}] - 112.4\mu\text{m}/\alpha) / t_{\text{react}} \quad (4)$$

(the unreacted layer is clearly still fully dense) and find that $p(\text{AR} + \text{MP}) = 14.3 \mu\text{m}/44.2 \mu\text{m} = 32.4\%$, which is a huge amount of porosity damage. In contrast, $p(\text{IHT} + \text{MP}) = 13.4 \mu\text{m}/61.1 \mu\text{m} = 21.9\%$, and $p(\text{HHT} + \text{MP}) = 13.4 \mu\text{m}/55.2 \mu\text{m} = 24.3\%$, which are less than the porosity damage of AR + MP. This proves quantitatively that the initial damage of metal foils during MP is much reduced by prior heat treatment. This is further verified by the huge inhomogeneity in the reacted layer thickness $\sigma[t_{\text{react}}(\text{AR} + \text{MP})] = 7.2 \mu\text{m} \gg \sigma[t_{\text{react}}(\text{IHT} + \text{MP})] \approx \sigma[t_{\text{react}}(\text{HHT} + \text{MP})] = 1.3 \mu\text{m}$, due to the more violent stress accumulation and cracking in AR + MP.

The AR + MP (44.2 μm reacted layer on 68.4 $\mu\text{m Al}_{\text{FCC}}$ layer), IHT + MP (61.1 μm reacted layer on 51.8 $\mu\text{m Al}_{\text{FCC}}$ layer) and HHT + MP (55.2 μm reacted layer on 55.1 $\mu\text{m Al}_{\text{FCC}}$ layer) that are mechanically prelithiated with the same amount of lithium ($\sim 4.65 \text{ mAh cm}^{-2}$) are then paired against LiFePO_4 cathode with an areal capacity of 2.65 mAh cm^{-2} , which means $\sim 1.8 \times$ excess Li inventory in the anode. The full-cell electrochemical performance is evaluated in a voltage range of 2.0–3.8 V. From Fig. 4a, it can be seen that while the voltage plateau exhibits a similar value for AR and AR + MP/IHT + MP/HHT + MP foil anodes, some variation in ICE is observed. Specifically, ICE of IHT + MP sample reaches 90%, approaching that of commercial graphite anode (92%). When contrasting the voltage profiles of the four samples, it is interesting that compared to AR and AR + MP samples, the overpotential of thermally treated samples (both IHT + MP and HHT + MP samples), is obviously increased, which may cause relatively lower capacity in the first cycle, when under the test condition of fixed cut-off voltage [17]. We speculate such difference in the initial internal resistance originated from reduced lithium transportation paths. That is to say, through thermal treatment, the amount of dislocation will decrease and grain boundary will increase, but generally, the total amount of defects that can serve as transportation channel for lithium ions will decline, resulting in a higher internal resistance in the first “formation” cycle. Therefore, a larger overpotential can be obviously observed in the thermally treated samples, especially when the annealing temperature increases as demonstrated in Fig. 4a. However, if the internal resistance of the treated sample remains invariably large during the whole 1st charging process, the general trend of voltage-capacity curves would not differ much from that of untreated sample. In fact, some aberration occurs in the later lithiation in the 1st cycle, and the slower ascent in voltage indicates a decrease in internal resistance, which is also verified in the in-situ EIS measurement in Fig. S10a, where some drop of internal resistance could be obviously observed, especially at the high voltage regime. We think such decrease in the internal resistance is closely associated with the generation of free volume (perhaps at nanoscale in the beginning). As discussed in this paper, during lithiation, the concomitant volume change will provoke gentle GB sliding that subsequently induces extra free-volume to allow faster Li atom (neutral) GB diffusion, reducing the internal resistance at the high voltage regime of the 1st charging curve as shown in Fig. S10b (purple curve). Note that

these initial microstructure adjustments have accumulated to such level as to tolerate the whole lithiation process in subsequent cycles. Thus, the 2nd, 5th, 10th and 20th voltage-capacity curves of IHT + MP samples show more stability (Fig. S10b).

Regarding long-time cycling (Fig. 4b), the AR + MP sample shows the worst cycle stability among the three MP samples, and sharply degraded after 40 cycles. In contrast, the IHT + MP sample achieves an average CE of 99.7% and maintains an 80% capacity retention (corresponding to an areal capacity of 2.12 mAh cm^{-2}) after 100 cycles, implying optimized heat treatment of Al foil anode could effectively promote the LDD in electrochemical cycling. Interestingly, the HHT + MP sample with less GBs density than IHT + MP sample, shows intermediate LDD, better than AR + MP but worse than IHT + MP. Such a ranking in LDD coincides well with the GB density before MP, as well as the reacted layer depth after MP:

$$t_{\text{react}}(\text{IHT} + \text{MP}) = 61.1 \mu\text{m} > t_{\text{react}}(\text{HHT} + \text{MP}) = 55.2 \mu\text{m} \gg t_{\text{react}}(\text{AR} + \text{MP}) = 44.2 \mu\text{m} \quad (5)$$

The LDD ranking does not agree with the ranking in total dislocation density before MP, proving unequivocally that sliding GBs is the controlling kinetic factor during MP and LDD.

To get an in-depth insight into the degradation mechanism as well as comprehensive understanding of the difference in electrochemical performance, postmortem examination is carried out to characterize the evolution of structural damage in the metallic foil anode with cycling. From surface and cross-sectional SEM images of AR + MP foil anode after 40 cycles in Fig. 4c, severe pulverization is evidently observed and some unreacted areas exist near the pulverization region, as marked by the dashed line. We anticipate such uneven electrochemical lithiation/delithiation mainly originated from the EL caused by huge cracks generated from lithiation shock during MP process. In contrast, IHT + MP sample with denser GB network shows excellent electrochemical ductility. Since more GB sliding system operated to alleviate phase transition stress, it reduced the tendency of GBs cracking so that a flat surface with less dead particles can be observed (Fig. 4d) after 40 cycles. By analyzing the electrochemical performance and the degradation mechanism, which confirms that the metallic foil with denser GB network is more capable of accommodating the initial lithiation shock as well as obtaining a uniform lithiation/delithiation, we can conclude that GB sliding is an important stress-relief mechanism to accommodate the phase transformation strains and the denser GB network allows deeper reaction layer (thus more uniform in the thickness direction) and better stress relief globally and reduce the tendency to cracking and electrolyte infiltration.

Furthermore, XPS characterization on the surface of cycled IHT + MP anode is carried out to understand the SEI formation mechanism. As demonstrated in Fig. S11, XPS analysis indicates that SEI formed on the anode mainly consists of common carbonaceous species, for example, C–C, C–O, C=O, inorganic lithium salts including Li_2CO_3 and LiF, the decomposition products of LiPF_6 which can be confirmed by P–F signal, and specifically, some reaction products involving Al–Li–O. It is widely acknowledged that electrolyte decomposition involves different bond cleavages, certainly resulting in the production of various radicals, which might further corrode Al on the surface, generating Al–Li–O in SEI. In contrast, from XPS spectrum, both Li_2O and Al_2O_3 peak are detected after mechanical prelithiation. It is worth mentioning that the existence of oxides on surfaces seems to have negligible influence on electrochemical performance, as revealed in Fig. S12b.

The question of electronic percolation to the active metal is intimately related to the “damage state” of the metallic foil. The $e^-(\text{metal})$ needs to reach grains by hopping across GBs, as grains are all surrounded by them and initially all of these corresponding GBs have no problem allowing $e^-(\text{metal})$ to conduct across. However, with repeated volume expansion and shrinkage, some of these GBs come apart, allowing partial or complete liquid electrolyte infiltration. This would decrease the

ability of $e^-(\text{metal})$ to hop across those GBs, so that we can monitor the “damage state” of the freestanding metallic foil anode in real time by testing its electronic ohmic resistance during cycling. Here, in order to quantitatively determine the “damage state” in terms of loss of electronic percolation, or increase of internal resistance, a three-electrode pouch cell prototype is implemented as illustrated in Fig. 5a. During battery cycling experiment, electrode A (negative electrode) and B (positive electrode) are used for routine charging/discharging, and after every two cycles, we apply a small voltage across electrode A (negative electrode) and C (negative electrode), calculating the resistance across the anode foil by reading the current from the multimeter (Ohm’s Law). As shown in Fig. 5b, both kinds LiAl_y foil beginning with a low in-plane resistance $< 1\Omega$. Due to the large phase transition stress, lithiation process at room temperature is bound to cause damage and change in the GB electrochemical complexions. That would lead to the resistance of the reaction layer to be much higher than Al_{FCC} layer in $\text{LiAl}_{\text{cubic}}/\text{Al}_{\text{FCC}}$ sheets which is equivalent to a parallel connection of a resistor and a conductor. So at the beginning, we measured almost the resistance of the unreacted Al_{FCC} layer. According to the laws of resistance:

$$R = \rho L/S \quad (6)$$

where R is the resistance, the ρ is resistivity of the material, the L and S stand for the length and cross-sectional area of the material respectively. The S of Al_{FCC} layer in IHT + MP sample is smaller than the AR + MP sample, so that the AR + MP sample has a relatively lower resistance than the intermediately IHT + MP one at first several cycles. After the

8th cycle, the resistance of control sample shows faster increase trend, because its Al_{FCC} layer is more prone to stress-buildup induced cracking which is consistent with what we discussed above: denser GB network relieves stress buildup and has reduced the tendency to cracking and electrolyte infiltration which thus kept a stable electronic percolation during cycling.

Li diffusion is as important as electronic percolation for reaction $\text{Al} + \text{Li}^+ + e^-(\text{metal}) \rightarrow \text{LiAl}$ to continue to happen cycle after cycle. Thus, we have tested the Li diffusion ability of the LiAl_y foil by CV measurement at different scan rates ranging from $0.01-0.1 \text{ mV s}^{-1}$ at potential of $0-1.5 \text{ V}$ versus Li^+/Li (Figs. S13a and S13b). The Li diffusion ability can be represented by the diffusion coefficient. According to the Randles–Sevcik equation:

$$I_p = kn^{3/2} AD^{1/2} C\nu^{1/2} \quad (7)$$

where I_p is the peak current of the CV curve [A], the constant $k = 2.69 \times 10^5 \text{ C mol}^{-1} \text{ V}^{-1/2}$ at room temperature. n stands for the number of electrons in the alloying/dealloying process (herein $n = 1$). A is the anode area ($A = 1.13 \text{ cm}^2$). Here, Li^+ concentration $C = 1.269 \times 10^{-2} \text{ mol cm}^{-3}$ (Al foil are lithiated by 5 mAh cm^{-2}) and ν is the scan rate [V/s]. The relationship between I_p and $\nu^{1/2}$ can be seen as a linear curve:

$$y = ax + b \quad (8)$$

$$D = (a / kn^{3/2} AC)^2 \quad (9)$$

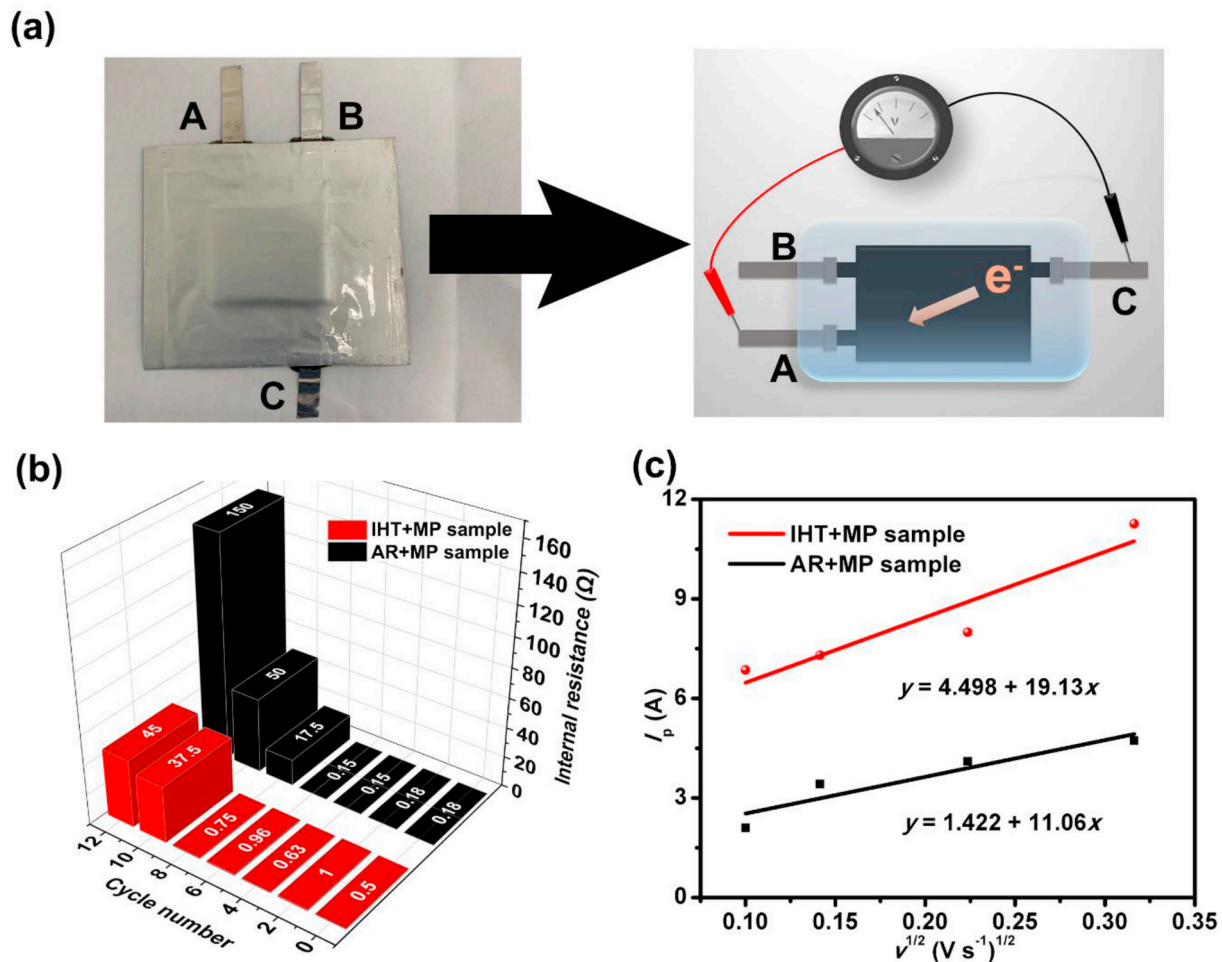


Fig. 5. Electronic percolation and Li diffusion measurements. a) Schematic illustration of the internal resistance test by a three-electrode pouch cell prototype. b) In-operando internal resistance test results at different cycle number and (c) maximum peak currents (I_p)-square root of scan rate ($\nu^{1/2}$) curve of IHT + MP and AR + MP samples.

The calculation result of diffusion coefficient is shown in Fig. 5c, where $D_{\text{IHT+MP}}$ is calculated to be $2.456 \times 10^{-5} \text{ cm}^2 \text{ s}^{-1}$ and $D_{\text{AR+MP}}$ is estimated to be $8.209 \times 10^{-6} \text{ cm}^2 \text{ s}^{-1}$. Both $D_{\text{IHT+MP}}$ and $D_{\text{AR+MP}}$ are quite higher than that of Li diffusivity in pure Al ($D = \sim 10^{-14} \text{ cm}^2 \text{ s}^{-1}$) [18], confirming that the lithiation/delithiation process has changed the GB complexion which provides more free volume to enhance the Li diffusion ability. Also, a sharp GB network makes $D_{\text{IHT+MP}} > D_{\text{AR+MP}}$, even though the latter had larger total dislocation density. Therefore, a decent rate performance is found in the IHT + MP foil. As demonstrated in Fig. S14, when we set a current rate range of 0.15C, 0.3C, 1C and 2C (0.5 mA cm^{-2} , 1 mA cm^{-2} , 2.5 mA cm^{-2} and 5 mA cm^{-2}), a capacity retention of 100%, 93%, 83% and 60% is maintained, respectively.

In order to evaluate the performance of the free-standing LiAl_y foil in real industrial applications with parsimonious electrolyte, a double-sided IHT + MP LiAl_y foil (total thickness of $130 \mu\text{m}$ and $65 \mu\text{m}$ thick one side) was utilized and its electrochemical performance was compared with a $130 \mu\text{m}$ thick Li metal foil in $3 \text{ cm} \times 3 \text{ cm}$ pouch cell. Fig. 6a shows pictures of foil anode (left) and the pouch cell (right). Here, LiFePO_4 was used as cathode and the amount of electrolyte is limited to 8 g Ah^{-1} which is an industrially acceptable electrolyte amount in practical pouch cells. As shown in Fig. 6b, at a rate of 1C, the $\text{LiFePO}_4/\text{LiAl}_y$ pouch cell shows better electrochemistry cycling behavior than that with Li_{BCC} metal foil anode of equal thickness. Moreover, this anode would not have Li_{BCC} metal dendrite growth problem, due to its higher voltage of $\sim 0.2 \text{ V}$ vs. Li^+/Li , even when cycling at high rates. Thus, those metallic foil anodes other than lithium foil anode is competitive when used as anodes of Li-metal battery, considering the dendrite-free, low-cost processing and energy-dense features.

Lastly, we did a set of combustion tests of Li_{BCC} foil (Movie S2) and LiAl_y foil (Movie S3). When lithium foil was placed on the flame of an

alcohol lamp, its surface is instantly oxidized to black. Then it begins to melt at the 6s and eventually violently burns (Fig. 6c). In contrast, the LiAl_y foil has never experienced violent burning (Fig. 6d) indicating that alloying reduces the activity of lithium metal, which makes the LiAl_y foil a much safer candidate for Li metal battery. We believe this is caused by the reduced vapor pressure of Li (pure Li boils at $1330 \text{ }^\circ\text{C}$) and the formation of passivating Al_2O_3 which is dense and adherent on the surface of the LiAl_y foil. Moreover, puncture experiments were performed on cycled LFP// LiAl_y and LFP//Li pouch cells with capacity of $\sim 50 \text{ mAh}$. As shown in Fig. S15, after piercing, the temperature of LFP// LiAl_y pouch cell only increased by $0.08 \text{ }^\circ\text{C}$ (e.g. from $22.58 \text{ }^\circ\text{C}$ to $22.66 \text{ }^\circ\text{C}$) whereas the temperature of LFP//Li pouch cell has risen by $4.5 \text{ }^\circ\text{C}$ (from 22.56 to $27.06 \text{ }^\circ\text{C}$), which shows LiAl_y is obviously of less thermal-runaway risk. These safety and long-term cycling features on equal foil thickness footing means the prelithiated Al foils deserve more attention than pure Li metal foil as an alternative type of metallic foil anode for high-energy density rechargeable batteries.

4. Conclusion

In this work, we developed a facile and efficient mechanical prelithiation approach which requires no electrolyte, and the ICE was greatly improved from 70% to 90% after prelithiation. However, the Al metal foil anode still has deficient cycling performance, which we attribute to the insufficient number of grain boundaries that leads to poor LDD, characterized by the rapid loss in electronic percolation across the foil. If we regard each metallic grain of the contiguous foil to be the equivalent of an active powder particle in the slurry approach, then GBs play the dual role of the binder (as GB can transmit stress and holds adjacent grain together) and conductive agent, as it allows e^- (metal) to hop from one grain to another. Therefore, thermal annealing

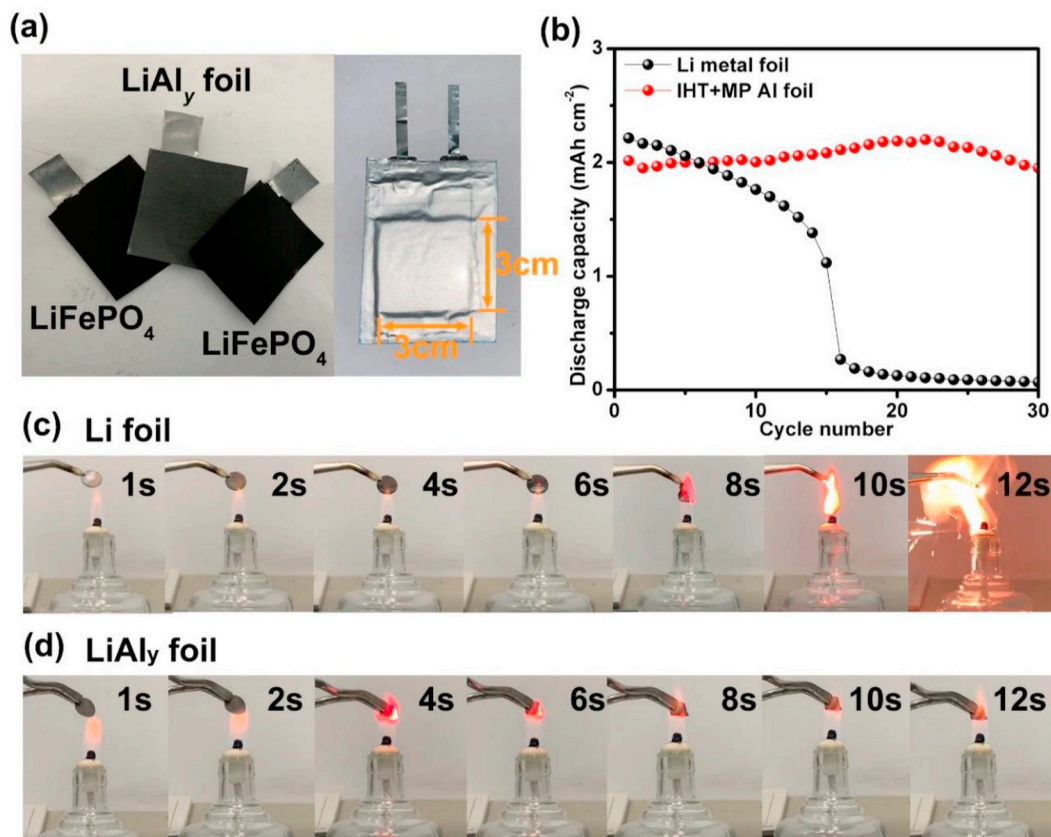


Fig. 6. Pouch cell and combustion test. a) Optical photograph of LiAl_y foil anode and the pouch cell (one pieces of double-sided IHT + MP LiAl_y foil and two pieces of single side LiFePO_4 cathode). b) Discharge capacity of LFP// LiAl_y and LFP//Li pouch cells. Combustion test of (c) Li foil and (d) LiAl_y foil.

and recrystallization, as a classic strategy to tune GB density, is adopted to optimize Al foil anode before mechanical prelithiation and full cell cycling in lithium-ion batteries. Based on the comparison of the microstructures and electrochemical performance at different thermal annealing condition, we realized that the GB density plays an essential role in stress relief and maintaining electron percolation during cycling. The GB complexion clearly evolves from more e⁻(metal) conducting to more Li-conducting with cycling, as electrolyte starts to invade along GBs. However, this process is gradual, and a foil with superior LDD will not easily generate dead grains with *all* surrounding GBs turning into complete electronic insulators. We quantitatively characterized the evolution of electron percolation by measuring the internal resistance of the foil anode, with a novel 3-electrode setup. When annealed at 300 °C for 15min, the Al foil anode shows slower in-plane electronic resistance growth and an excellent tolerance to volume change, and maintains 80% capacity retention after 100 cycles in LiFePO₄/LiAl_y full cell with 1.8 × excess lithium inventory. Additionally, the pouch-cell performance of free-standing IHT + MP LiAl_y foil is significantly better than that of pure Li_{BCC} foil of equal thickness, especially under lean-electrolyte condition, suggesting such safe, cheap and high energy density metallic foil anodes should deserve more of our attention besides lithium metal anode.

Declaration of competing interest

The authors declare that they have no known competing financial interests or personal relationships that could have appeared to influence the work reported in this paper.

Acknowledgements

This work was supported by funding from National Natural Science Foundation of China (NSFC-No. 51602222, 51632001 and 51972236); The authors are grateful for assistance by Dr Pengcheng Zhang from Xi'an Jiaotong University in Electron backscattering diffraction characterization. J.L. acknowledges the support by Wuxi Weifu and Samsung Advanced Institute of Technology.

Appendix A. Supplementary data

Supplementary data to this article can be found online at <https://doi.org/10.1016/j.nanoen.2019.104274>.

References

- [1] Y. Hamon, T. Brousse, F. Jousse, P. Topart, P. Buvat, D.M. Schleich, Aluminum negative electrode in lithium ion batteries, *J. Power Sources* 97–98 (2001) 185–187, [https://doi.org/10.1016/S0378-7753\(01\)00616-4](https://doi.org/10.1016/S0378-7753(01)00616-4).

- [2] S. Li, J. Niu, Y.C. Zhao, K.P. So, C. Wang, C.A. Wang, J. Li, High-rate aluminium yolk-shell nanoparticle anode for Li-ion battery with long cycle life and ultrahigh capacity, *Nat. Commun.* (2015) 1–7, <https://doi.org/10.1038/ncomms8872>.
- [3] X. Lei, C. Wang, Z. Yi, Y. Liang, J. Sun, Effects of particle size on the electrochemical properties of aluminum powders as anode materials for lithium ion batteries, *J. Alloy. Comp.* 429 (2007) 311–315, <https://doi.org/10.1016/j.jallcom.2006.04.019>.
- [4] G. Xu, Q. bo Yan, A. Kushima, X. Zhang, J. Pan, J. Li, Conductive graphene oxide-polyacrylic acid (GOPAA) binder for lithium-sulfur battery, *Nano Energy* 31 (2017) 568–574, <https://doi.org/10.1016/j.nanoen.2016.12.002>.
- [5] S. Li, M. Jiang, Y. Xie, H. Xu, J. Jia, J. Li, Developing high-performance lithium metal anode in liquid electrolytes: challenges and progress, *Adv. Mater.* 30 (2018) 1–29, <https://doi.org/10.1002/adma.201706375>.
- [6] M.W. Forney, M.J. Ganter, J.W. Staub, R.D. Ridgley, B.J. Landi, Prelithiation of silicon-carbon nanotube anodes for lithium ion batteries by stabilized lithium metal powder (SLMP), *Nano Lett.* 13 (2013) 4158–4163, <https://doi.org/10.1021/nl401776d>.
- [7] J. Zhao, Z. Lu, H. Wang, W. Liu, H.W. Lee, K. Yan, D. Zhuo, D. Lin, N. Liu, Y. Cui, Artificial solid electrolyte interphase-protected Li₂Si nanoparticles: an efficient and stable prelithiation reagent for lithium-ion batteries, *J. Am. Chem. Soc.* 137 (2015) 8372–8375, <https://doi.org/10.1021/jacs.5b04526>.
- [8] M.G. Kim, J. Cho, Air stable Al₂O₃-coated Li₂NiO₂ cathode additive as a surplus current consumer in a Li-ion cell, *J. Mater. Chem.* 18 (2008) 5880–5887, <https://doi.org/10.1039/b814161d>.
- [9] M. Jiang, Y. Yu, H. Fan, H. Xu, Y. Zheng, Y. Huang, S. Li, J. Li, Full-cell cycling of a self-supporting aluminum foil anode with a phosphate conversion coating, *ACS Appl. Mater. Interfaces* 11 (2019) 15656–15661, <https://doi.org/10.1021/acsami.9b02813>.
- [10] B. Qin, T. Diemant, H. Zhang, A. Hoefling, R.J. Behm, J. Tübke, A. Varzi, S. Passerini, Revisiting the electrochemical lithiation mechanism of aluminum and the role of Li-rich phases (Li_{1+x}Al) on capacity fading, *ChemSusChem* (2019) 2492, <https://doi.org/10.1002/cssc.201900597>.
- [11] W. Weibull, A statistical theory of the strength of materials IVA, *Ingenioersvetenskapskad. Handl.* 151 (1939).
- [12] W. Weibull, The phenomenon of rupture in solids, *IVA Handl.* 153 (1939).
- [13] F.J. Humphreys, M. Hatherly, *Recrystallization and Related Annealing Phenomena*, Elsevier, 2012.
- [14] H. Fan, S. Li, G. Pan, Y. Yu, H. Xu, M. Jiang, Y. Huang, J. Li, Air-stable Li_xAl Foil as Free-Standing Electrode with Improved Electrochemical Ductility by Shot-Peening Treatment, 2019. In-Press.
- [15] M. Fiebig, Y. Tokura, T. Kimura, J.C. Lashley, a P. Ramirez, S. Park, Y.J. Choi, C. L. Zhang, T. Arima, H. Katsura, N. Nagaosa, a V. Balatsky, I. a Sergienko, E. Dagotto, M. Mostovoy, a B. Harris, T. Yildirim, a Aharony, G. Lawes, N. Momozawa, Y. Yamaguchi, M. Mita, Y. Nagao, S. Utsumi, M. Abe, Observation of giant diffusivity, *Science* (80-.) (2008) 1646–1649, <https://doi.org/10.1126/science.1151771>.
- [16] J.W. Cahn, Y. Mishin, A. Suzuki, Duality of dislocation content of grain boundaries, *Philos. Mag.* 86 (2006) 3965–3980, <https://doi.org/10.1080/14786430500536909>.
- [17] Y. Zheng, Y. Wang, Y. Lu, Y.S. Hu, J. Li, A high-performance sodium-ion battery enhanced by macadamia shell derived hard carbon anode, *Nano Energy* 39 (2017) 489–498, <https://doi.org/10.1016/j.nanoen.2017.07.018>.
- [18] C. Moreau, A. Allouche, E.J. Knystautas, Measurements of the diffusion rate of lithium in aluminum at low temperature by elastic recoil detection analysis, *J. Appl. Phys.* 58 (1985) 4582–4586, <https://doi.org/10.1063/1.336250>.

Supporting information for

Optimal annealing of Al foil anode for prelithiation and full-cell cycling in Li-ion battery: the role of grain boundaries in lithiation/delithiation ductility

Yue Yu^{1,2}, Sa Li^{1,2*}, Huimin Fan^{1,2}, Hui Xu^{1,2}, Mengwen Jiang^{1,2}, Yunhui Huang^{1,2}, and Ju Li^{3*}

¹ School of Materials Science and Engineering, Tongji University, Shanghai 201804, China

² Institute of New Energy for Vehicles, Tongji University, Shanghai 201804, China

³ Department of Nuclear Science and Engineering and Department of Materials Science and Engineering, Massachusetts Institute of Technology, Cambridge, MA 02139, USA

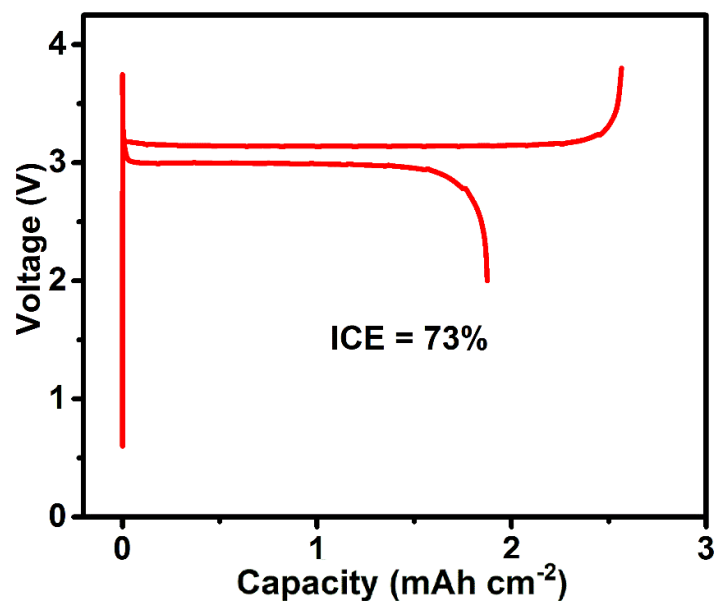


Fig. S1 The 1st cycle voltage-capacity profile of AR Al foil anode.

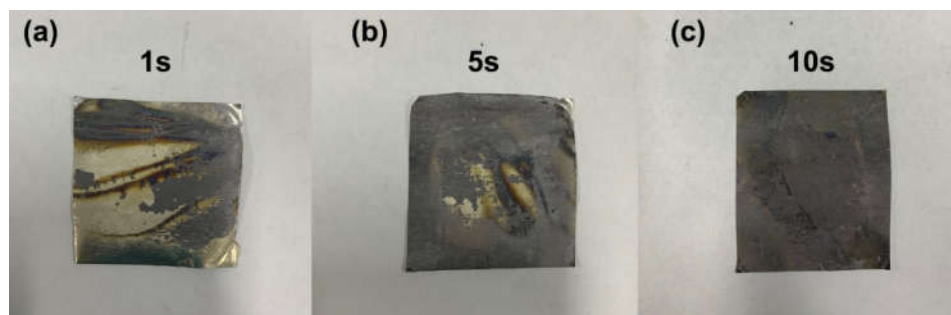


Fig. S2 The MP process treated for (a) 1s, (b) 5s and (c) 10s under 30MPa.

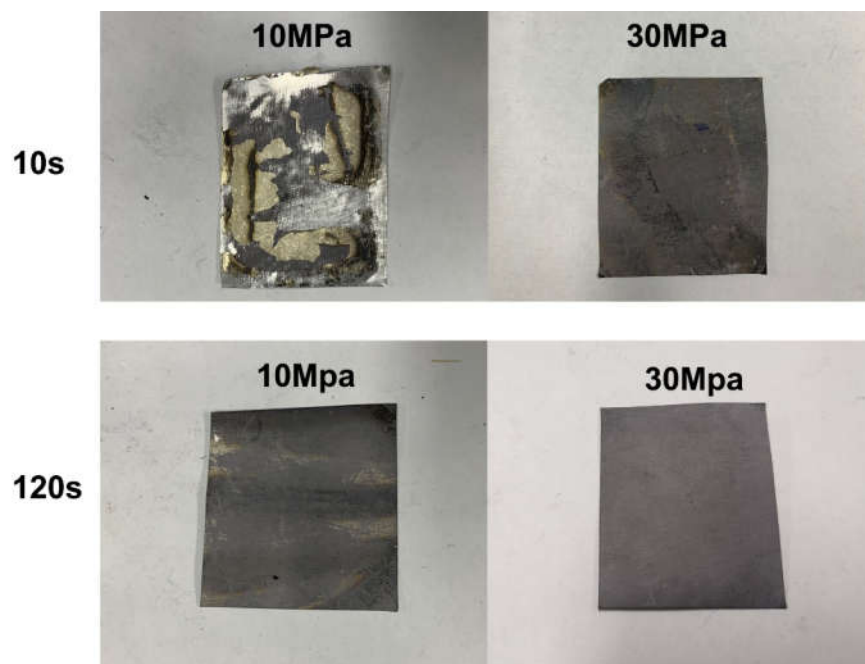


Fig. S3 Optical images of LiAl_y foil after MP under different pressures and press time.

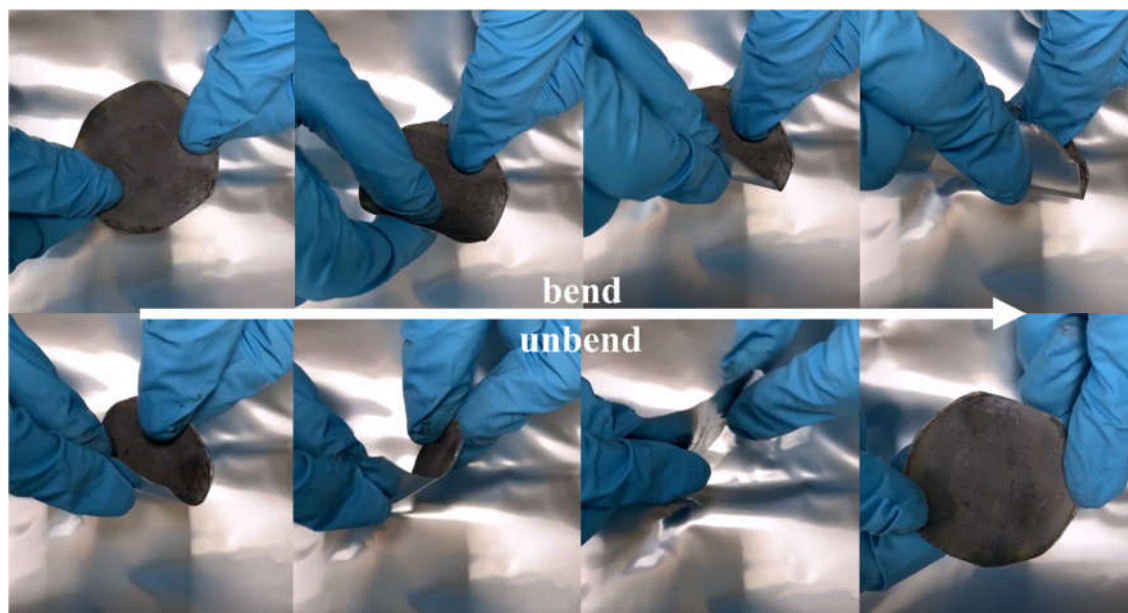


Fig. S4 The bending experiment of the LiAl_y foil.

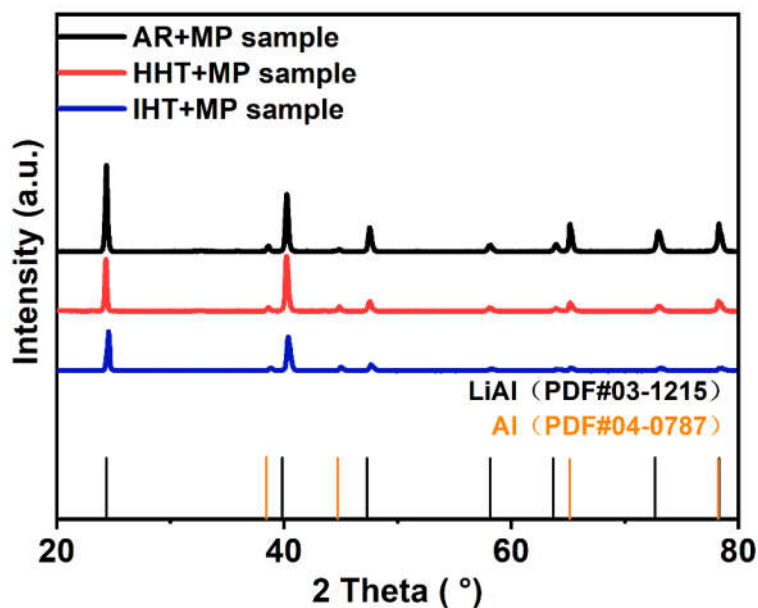


Fig. S5 The X-ray diffraction of the AR+MP, IHT+MP and HHT+MP sample.

We also examine the grain size of as-formed LiAl_y in AR, IHT and HHT samples through X-ray diffraction. According to Scherrer equation of $D = k\lambda / (\beta \cos \theta)$, where β is the peak width in radians at half-maximum intensity, D is the grain size, λ is the wavelength of the radiation (1.54056 Å for Cu K α radiation), k is the shape factor constant and θ is the peak position, and β ranking that $\beta_{\text{IHT+MP}} > \beta_{\text{HHT+MP}} > \beta_{\text{AR+MP}}$, we interestingly find that LiAl_y in IHT has the smallest grain among the three.

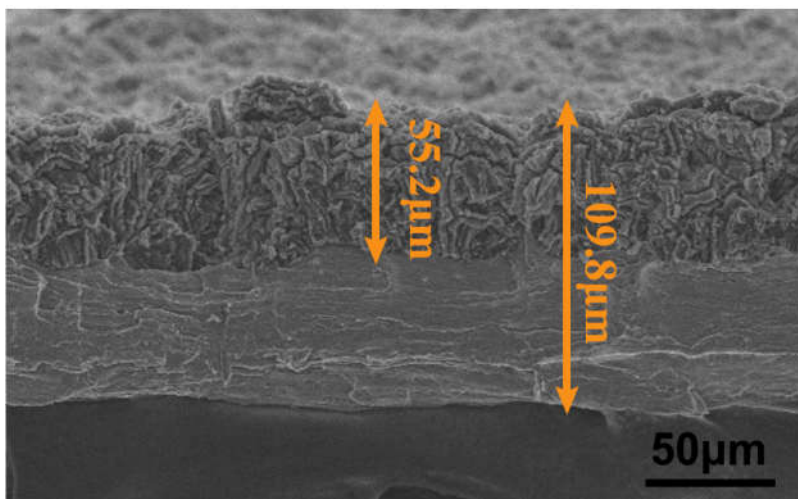


Fig. S6 The cross-sectional SEM image of HHT+MP LiAl_y foil.

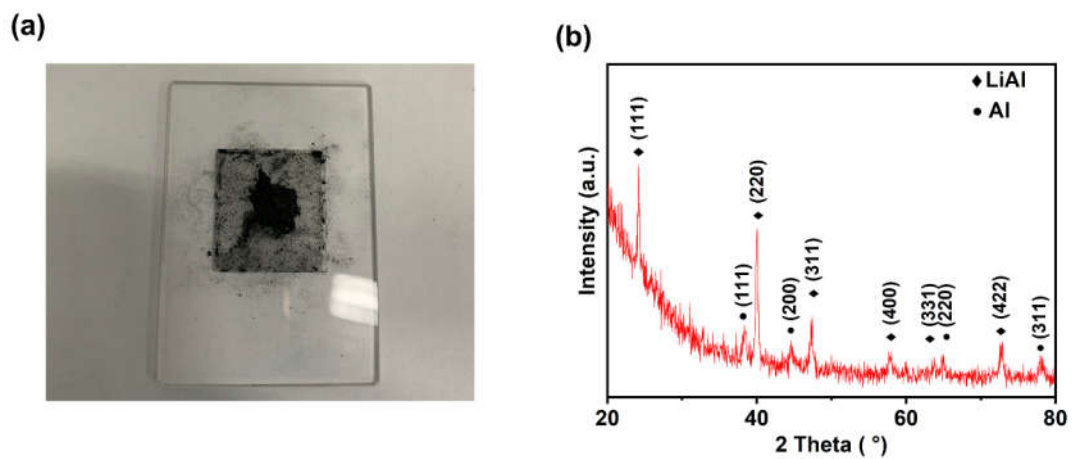


Fig. S7 (a) The LiAl_y fragments scratched from the foil. (b)The XRD characterization of the reaction layer on the LiAl_y foil.

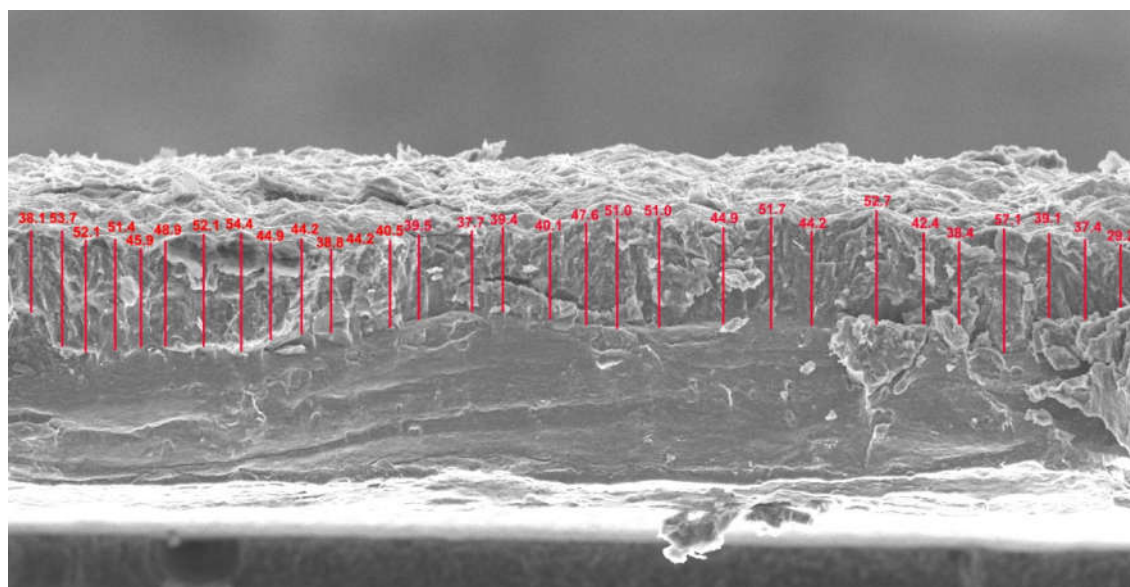


Fig. S8 Illustration of reaction layer thickness measurement.

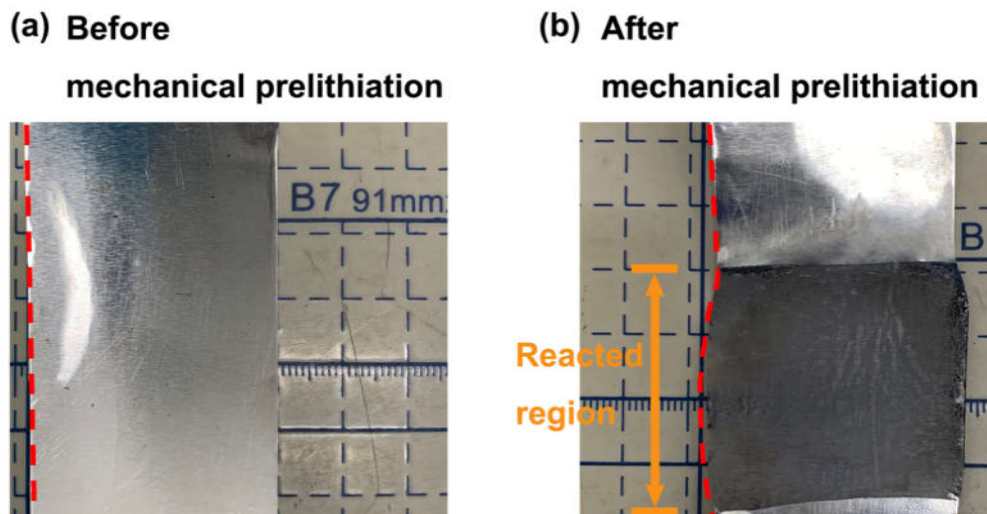


Fig. S9 Optical photographs of Al foil (a) before and (b) after MP process.

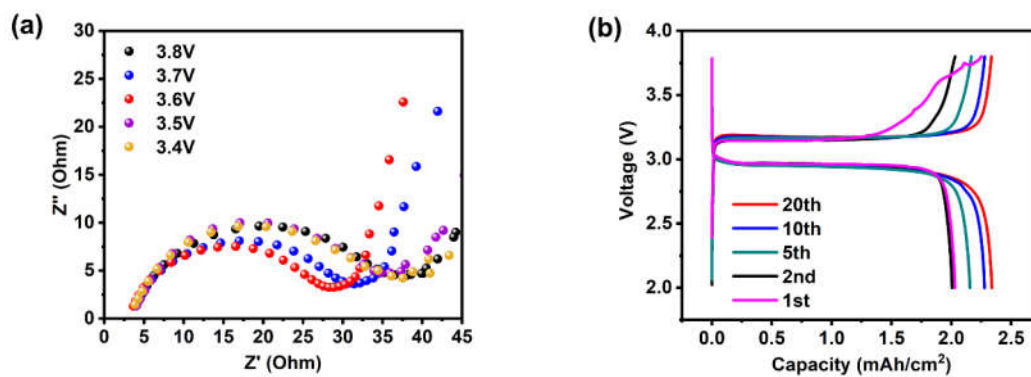


Fig. S10 (a) The EIS measurement of IHT+MP sample from 3.4V to 3.8V during first charge. (b) The voltage-capacity curve of IHT+MP sample.

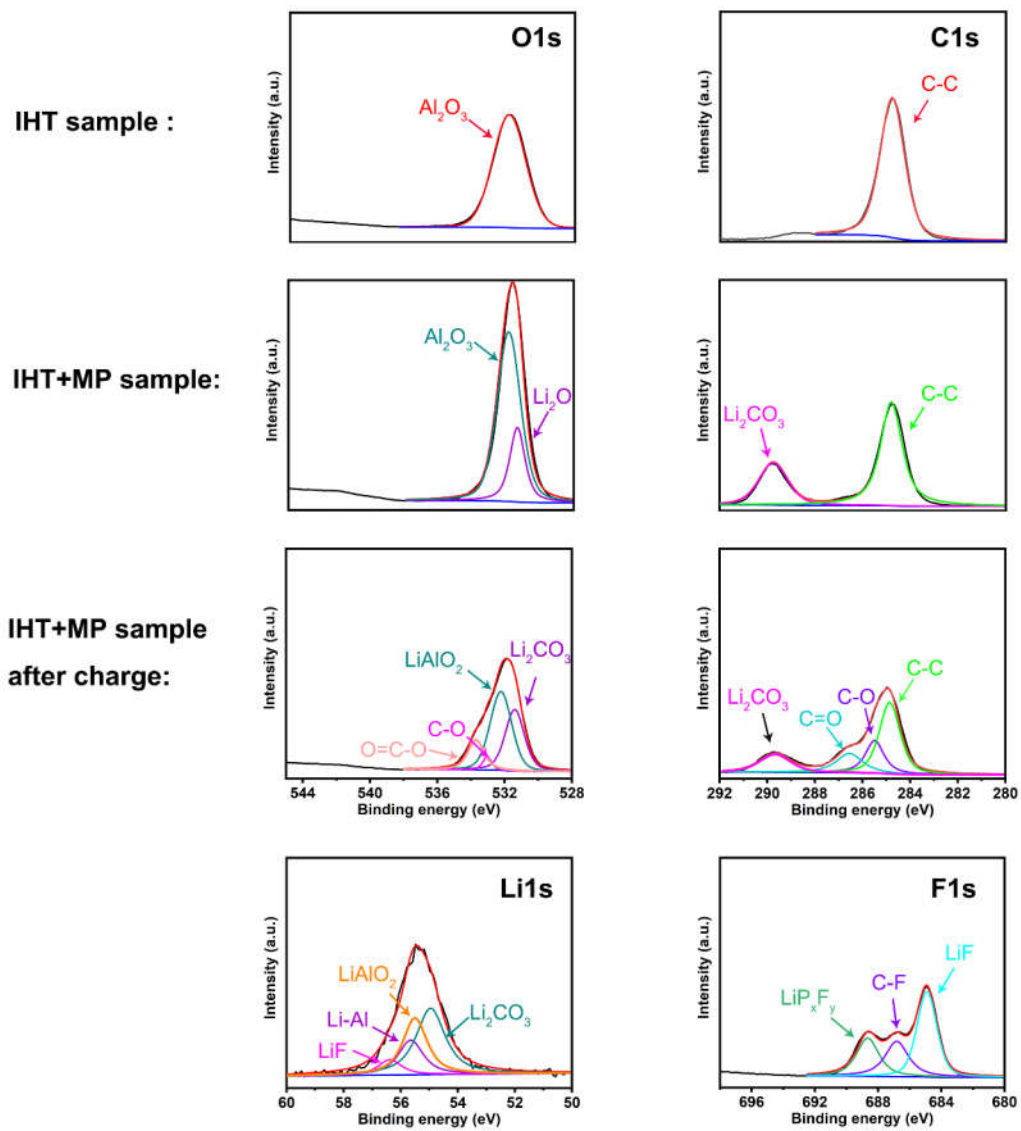


Fig. S11 XPS scans of the O 1s, C 1s, of the IHT sample (before cycle), IHT+MP sample (before cycle) and IHT+MP sample (after charge) respectively. And XPS scans of the Li 1s, F 1s of the IHT+MP sample (after charge).

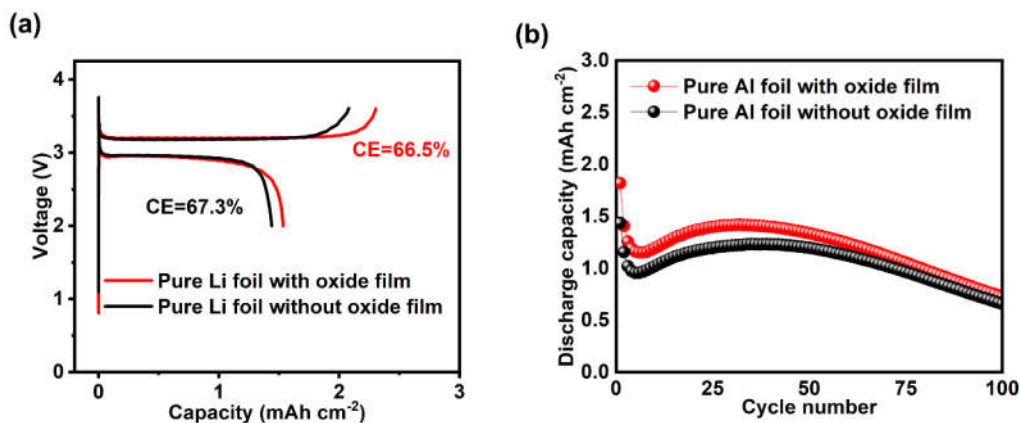


Fig. S12(a)The Voltage-Capacity curve and (b)cycle performance of IHT Al foil with/without oxide film.

We eliminate the oxide film by polishing the IHT Al foil in glove box filled with Ar atmosphere. From Fig. S12a, the identical voltage plateaus are observed for both samples, indicating the same electrochemical reactions that involves no Al₂O₃ layer occurs. Meanwhile, the cycle performance in Fig. S12b also reveals that the Al₂O₃ layer that is usually several nanometers thick has little effect on electrochemical performance.

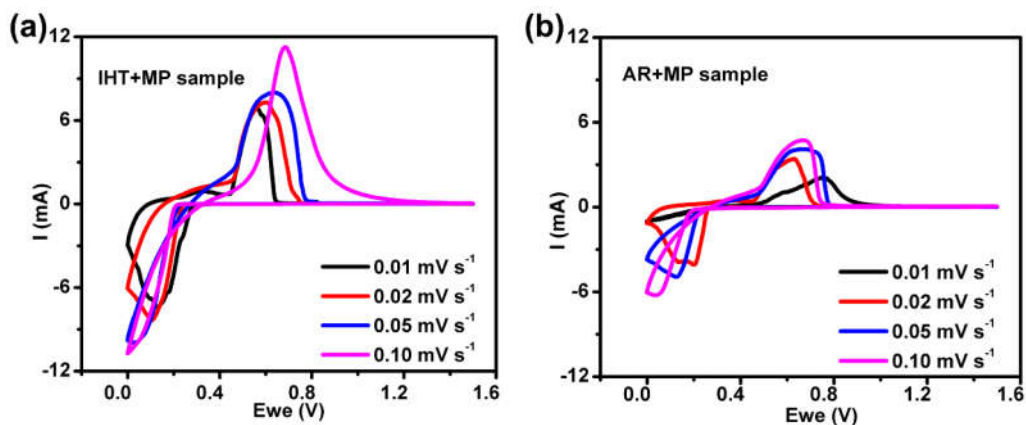


Fig. S13 The cyclic voltammetry (CV) curves of (a) IHT+MP sample and (b) AR+MP sample.

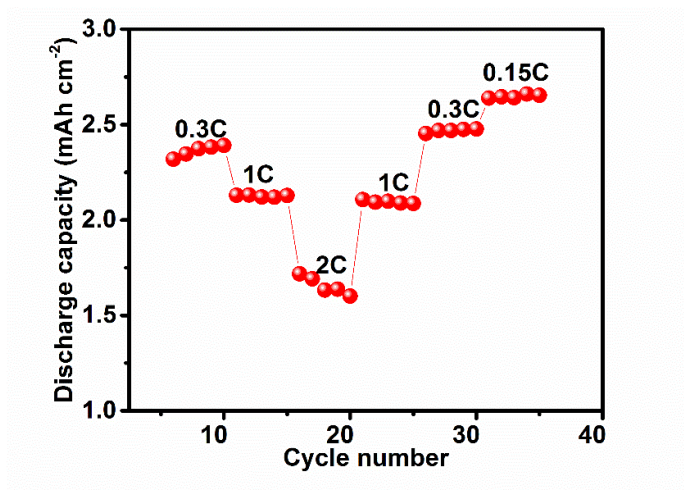


Fig. S14 The rate performance of IHT+MP sample.

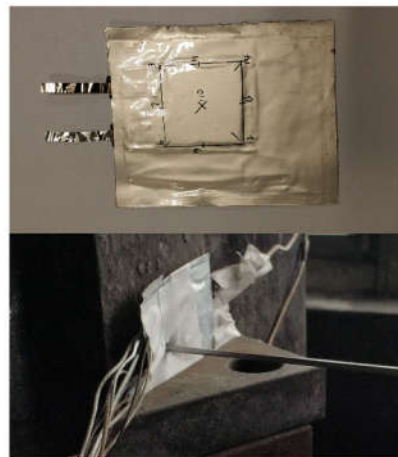
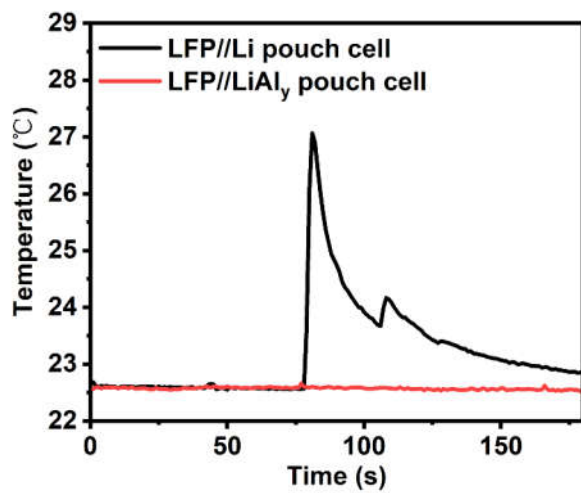


Fig. S15 Temperature changes of LFP//Li and LFP//LiAl_x pouch cell during puncture experiments and optical photo of the puncture experiments.

Table S1 Thickness (μm) measurement result of the reacted layer of AR+MP sample

Thickness (μm) of the reacted layer					Average thickness	Variance	Reacted layer thickness t_{react}
38.11	54.42	51.05	44.26	37.43	44.96 μm	6.63 μm	44.96 \pm 6.63 μm
53.75	39.79	38.78	52.73	29.25			
44.22	39.49	47.63	42.38	52.06			
51.38	37.77	51.01	38.44	52.06			
45.94	39.46	44.89	57.16	44.89			
48.98	40.13	51.76	39.12	40.51			

Table S2 Lateral areal expansion of the three samples during MP

Sample	AR+MP	IHT+MP	HHT+MP
Lateral areal expansion	11.0%	15.5%	16.5%

Movie. S1:

bending and winding test: <http://li.mit.edu/S/YueYu/Upload/bending.mp4>

Movie. S2:

Combustion tests of Li foil: <http://li.mit.edu/S/YueYu/Upload/Li-foil.mp4>

Movie. S3:

Combustion tests of LiAl₂ foil: [http://li.mit.edu/S/YueYu/Upload/LiAl₂-foil.mp4](http://li.mit.edu/S/YueYu/Upload/LiAl2-foil.mp4)